Limb-Darkening Observations Testing State-of-the-Art Model Atmospheres

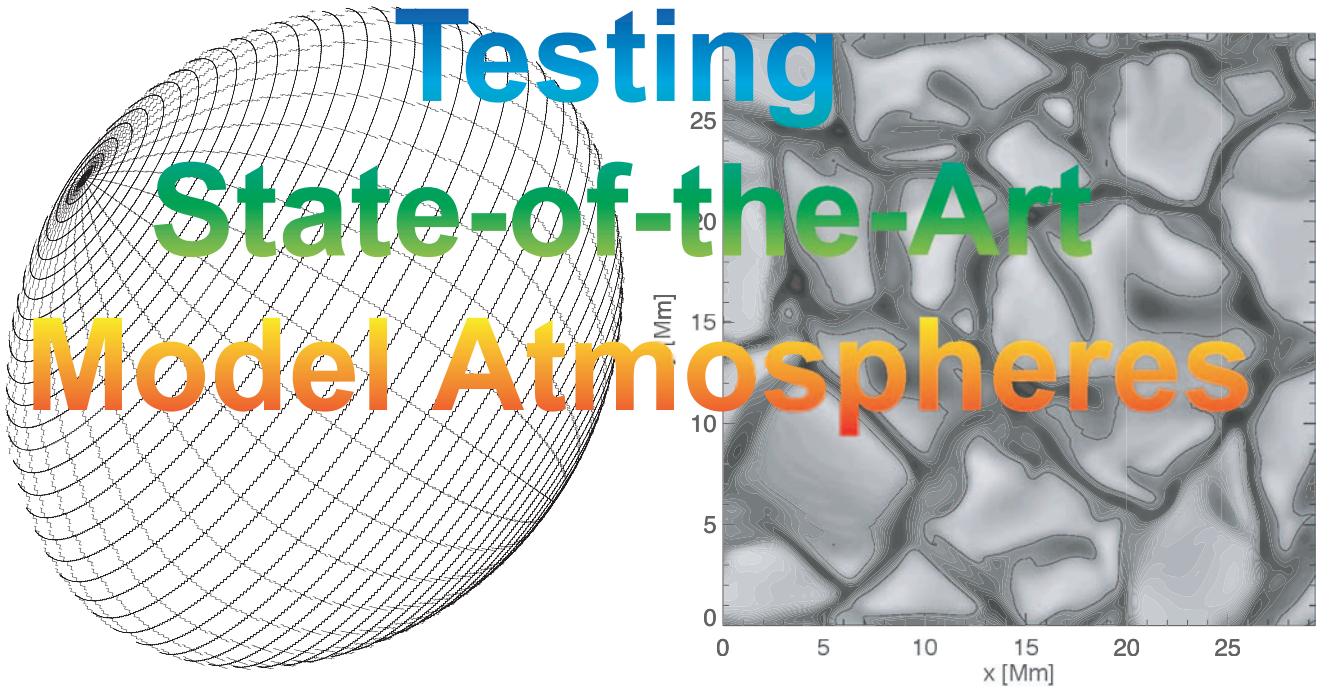

Jason Aufdenberg

Michelson Postdoctoral Fellow
National Optical Astronomy Observatory
Tucson, USA

Interferometry Collaborators

S. T. Ridgway (NOAO)

P. Kervella, A. Mérand, V. Coudé du Foresto,

E. Di Folco, G. Romero

(LESIA, Observatorie de Paris-Meudon)

O. Absil (Université de Liège)

H. McAlister and the CHARA Team

(Georgia State University and Mount Wilson Observatory)

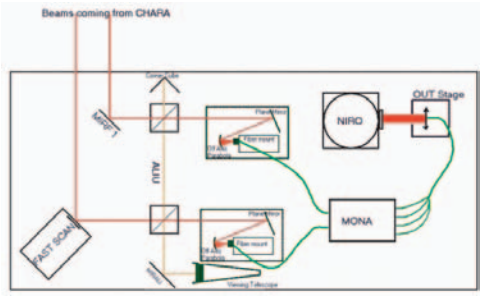

Model Atmosphere Collaborators

H.-G. Ludwig (Observatorie de Paris-Meudon)

P. Hauschildt, A. Schweitzer (Hamburger Sternwarte)

F. Allard (CRAL-ENS, Lyon)

E. Baron (University of Oklahoma)

T. Barman (UCLA)

What's to Come....

Vega's Gravity Darkening with CHARA/FLUOR

Procyon's Convection with VLTI/VINCI and Mark III

Schematic Two-Telescope Interferometer

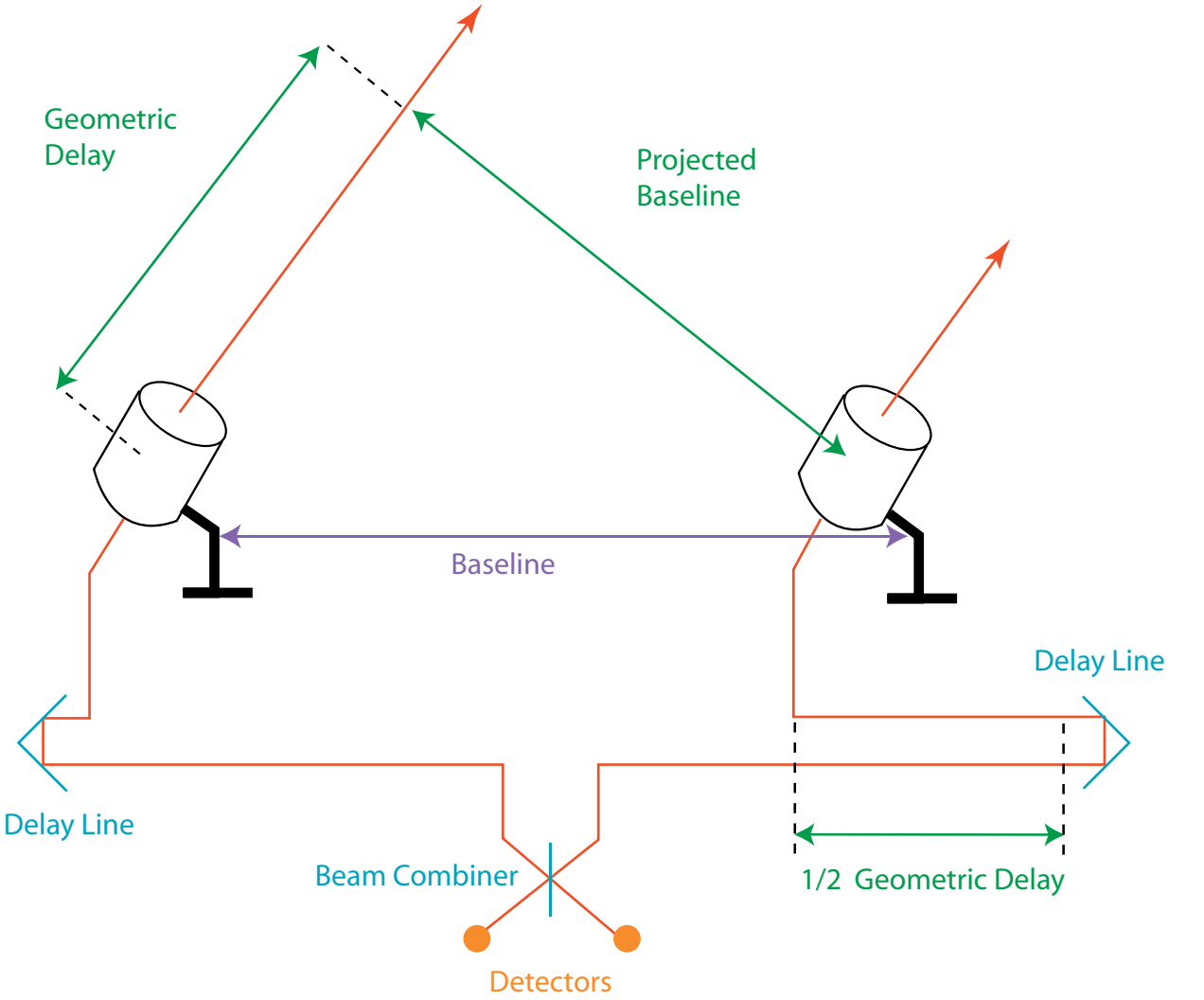

adapted from Oskar van der Lühe

The Observable: Visibility

$$V = \frac{I_{max} - I_{min}}{I_{max} + I_{min}}$$

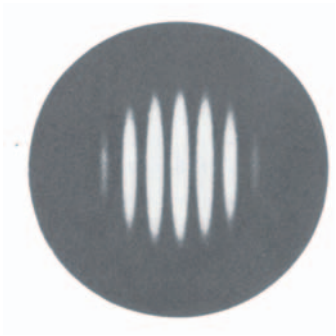

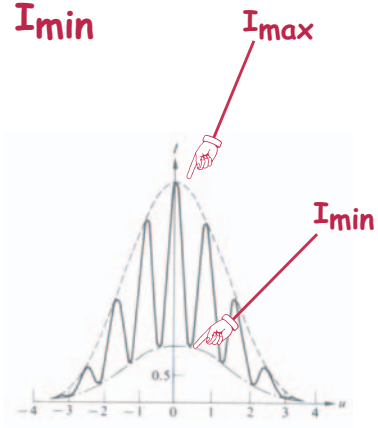

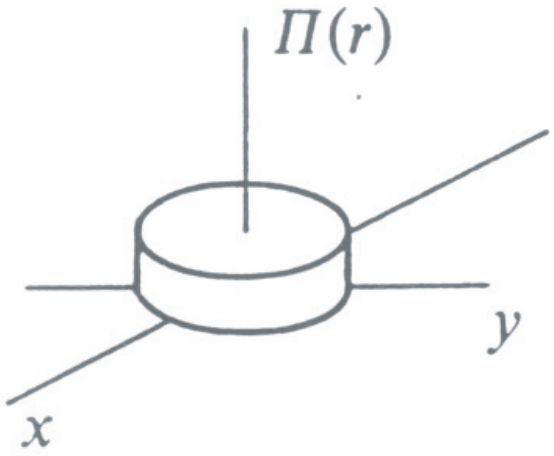

on the sky

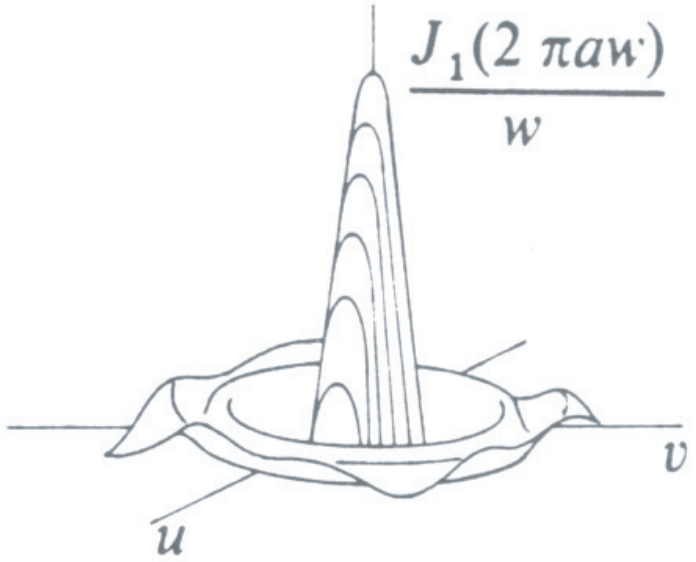

what the interferometer measures

Limb Darkening Basics

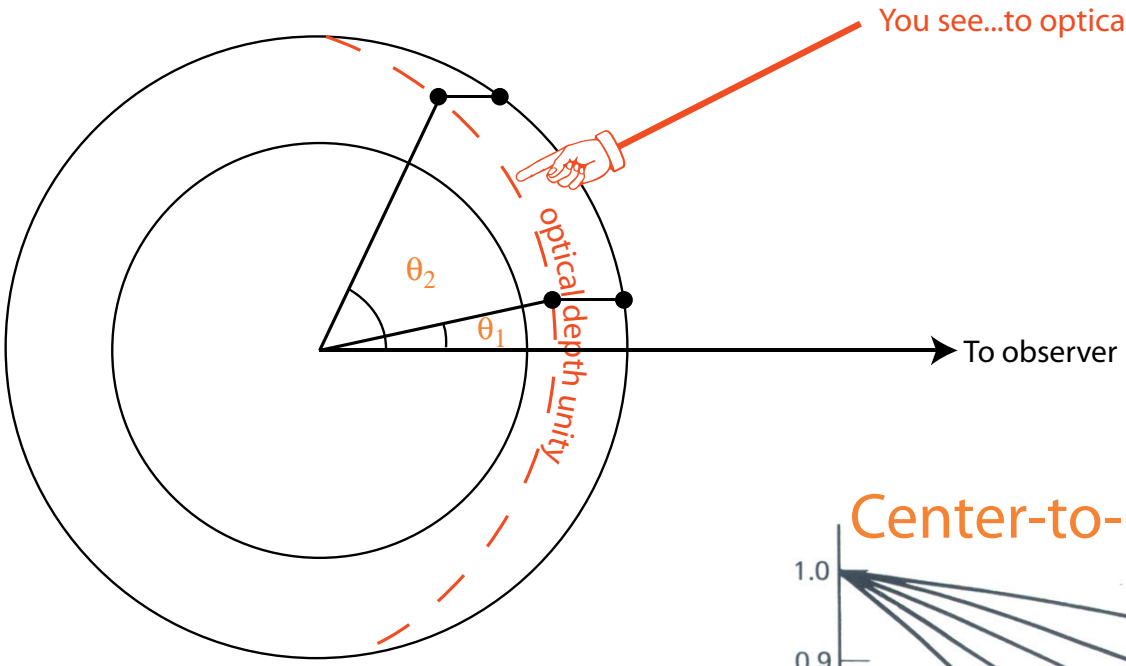

$$B_\lambda = 2\ ckT\ \lambda^{-4}$$

$$\frac{dB_\lambda}{dT} = \frac{2}{c}k\ \lambda^{-4}$$

Center-to-Limb Intensity Profile

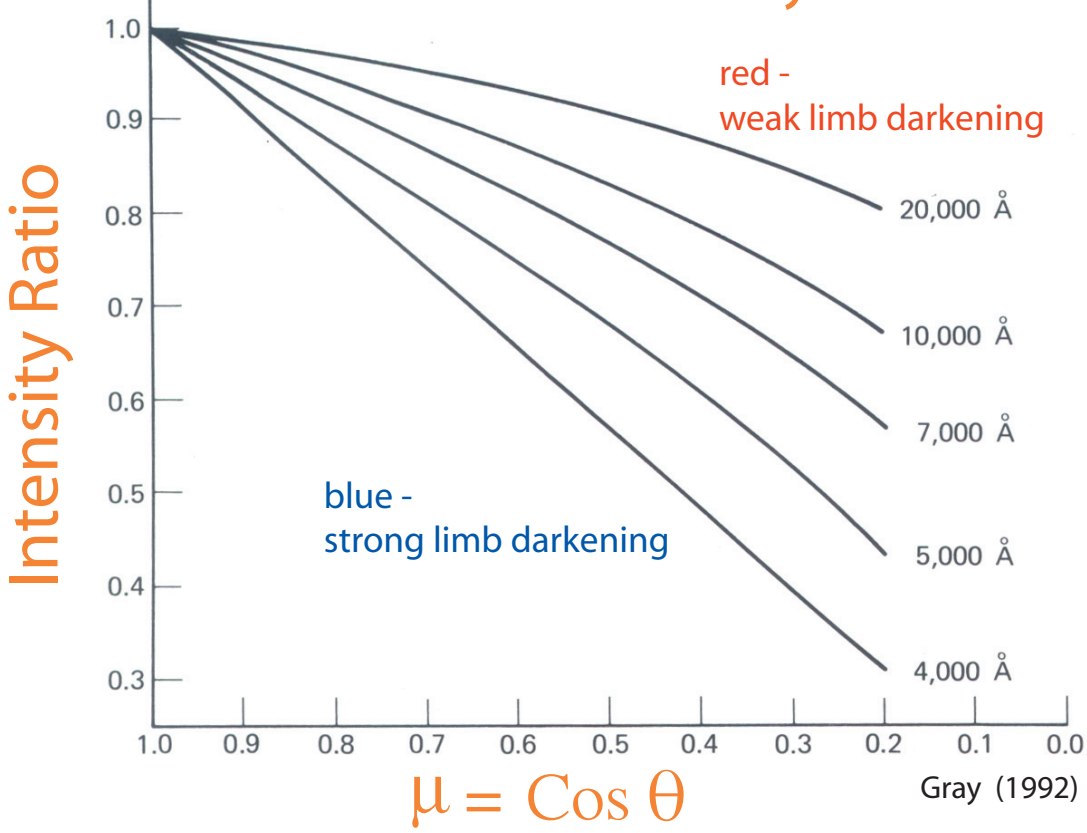

Gray (1992)

“Direct” Limb darkening measurements from interferometry

M5 II	α Her (Perrin et al., 2004)
M4.5 III	BY Boo (Wittkowski et al., 2001)
M4 III	V416 Lac, ψ Phe (Wittkowski et al., 2001; Wittkowski et al., 2004)
M1Iab	Betelgeuse (a Ori; Burns et al., 1997; Perrin et al., 2004)
M0 III	γ Sge (Wittkowski et al., 2001)
K2 III	α Ari (Hajian et al., 1998)
K1.5 III	Arcturus (α Boo; Quirrenbach et al., 1996)
K0 III	α Cas (Hajian et al., 1998)
A7 V	α Aql (Ohishi et al., 2004)
A1 V	Sirius (α CMa; Hanbury Brown et al., 1974)

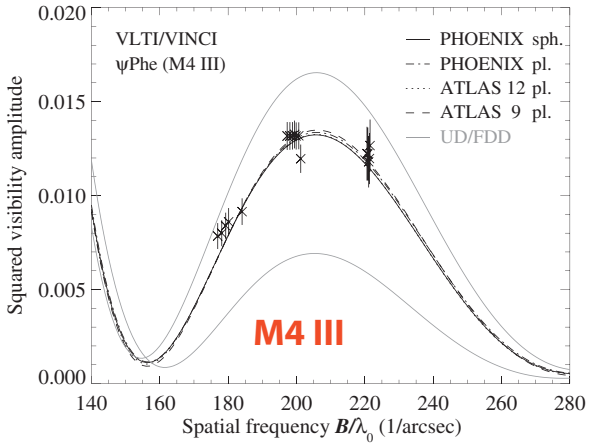

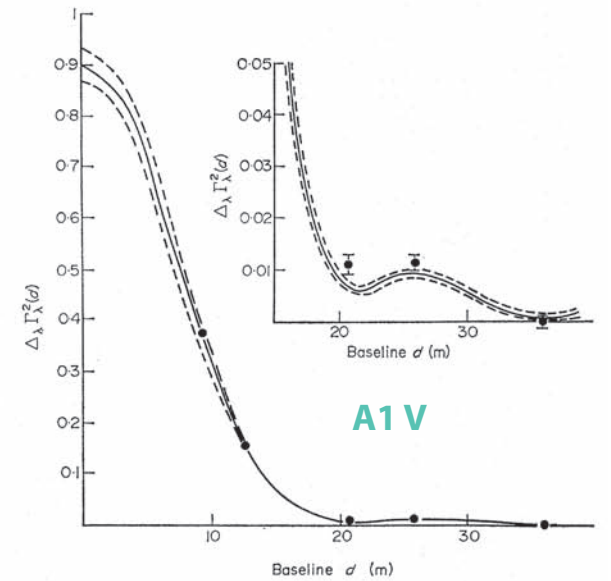

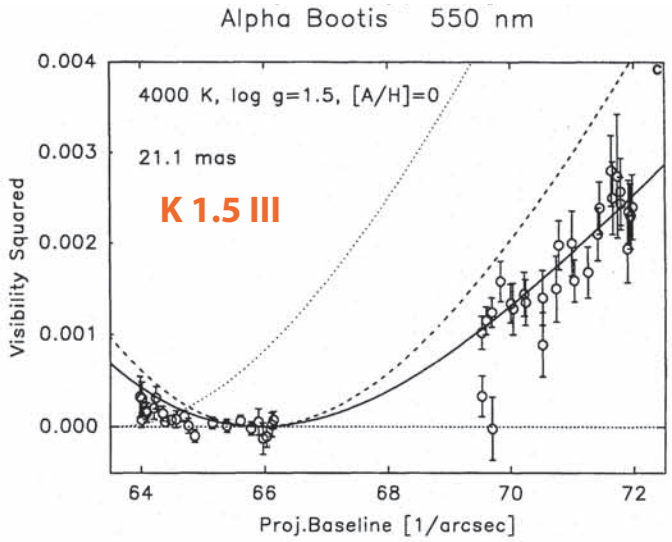

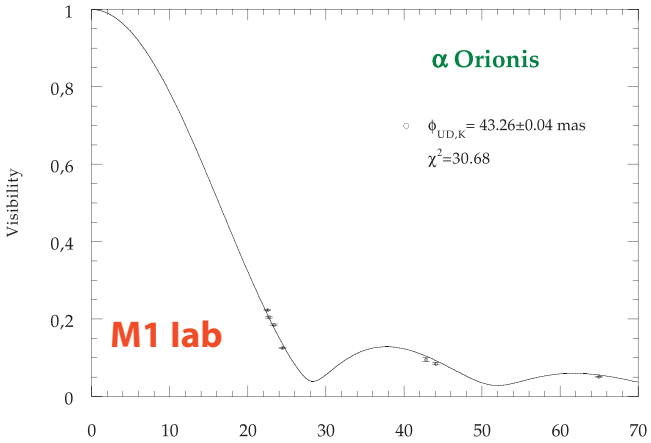

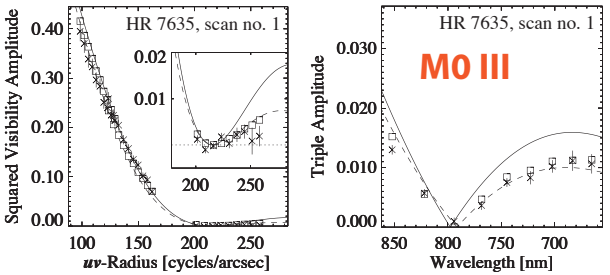

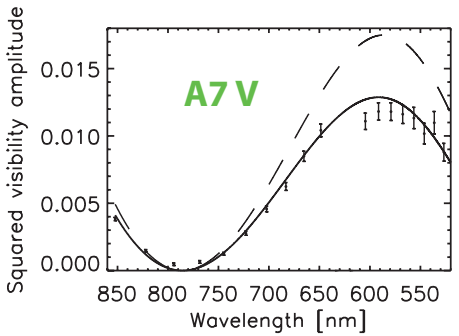

Vega

Vega as *the* photometric standard star (1862 -)

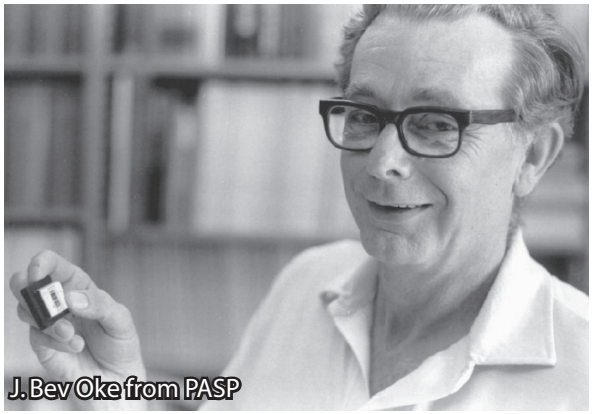

A. Code and J. B. Oke put Vega and other stars fluxes into absolute units (1960)

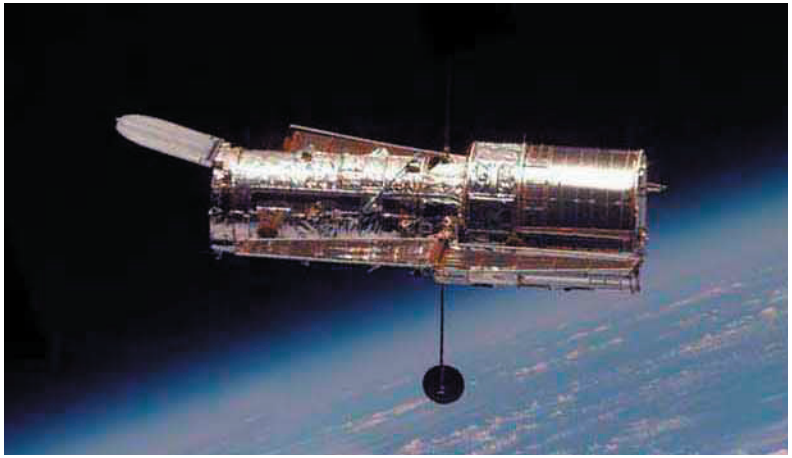

Vega with HST/STIS (Bohlin & Gilliland, 2004)

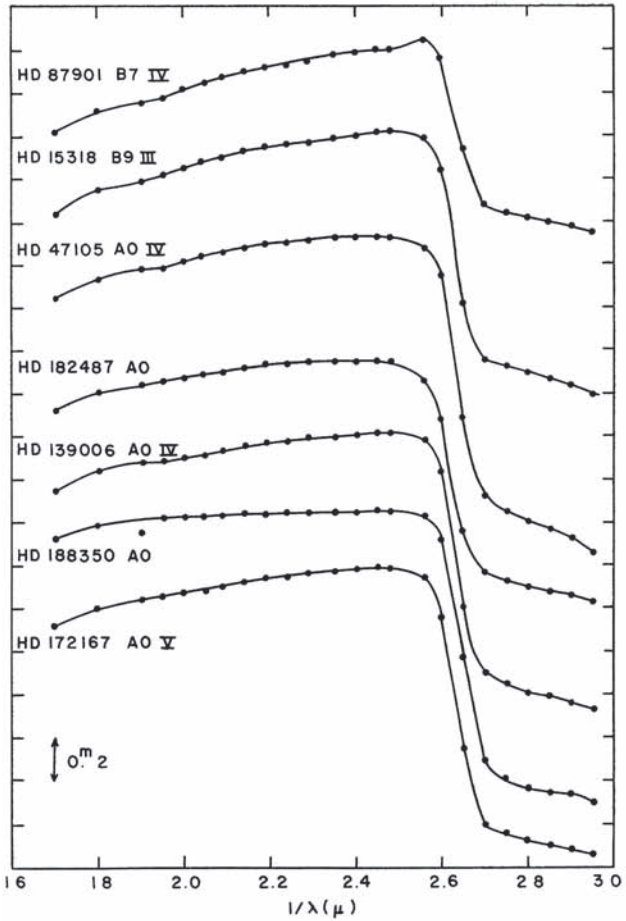

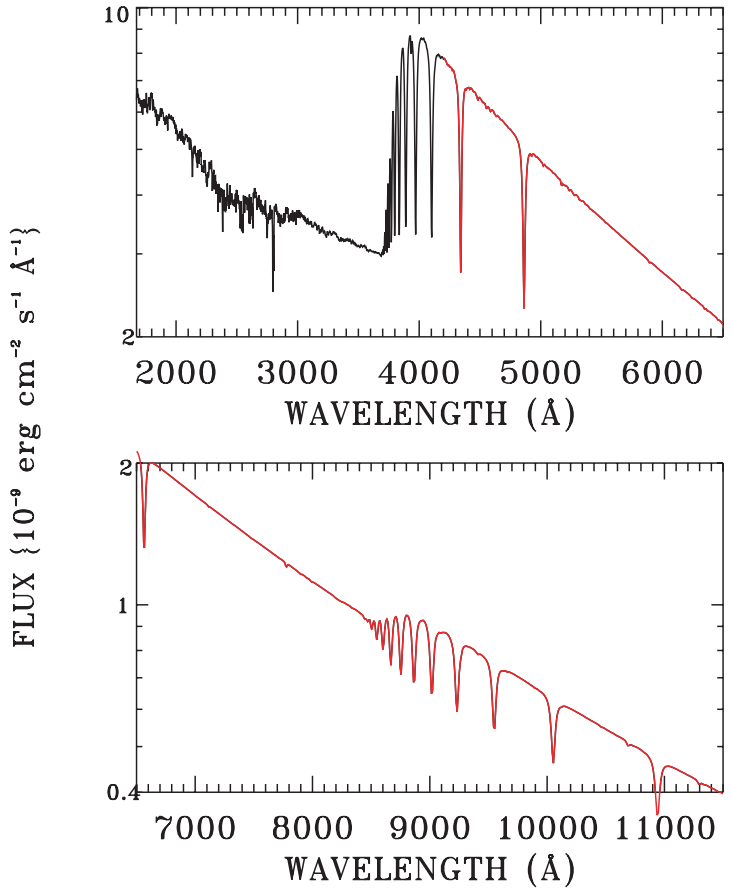

Vega is 60% larger (in Radius) than Sirius. Mass-Radius relation predicts ~12%.

R (Vega) = 2.73 ± 0.01 $R_\odot$ (Ciardi et al. 2001)

R (Sirius) = 1.711 ± 0.013 $R_\odot$; Mass (Sirius) = 2.12 ±0.06 $M_\odot$ (Kervella et al. 2003)

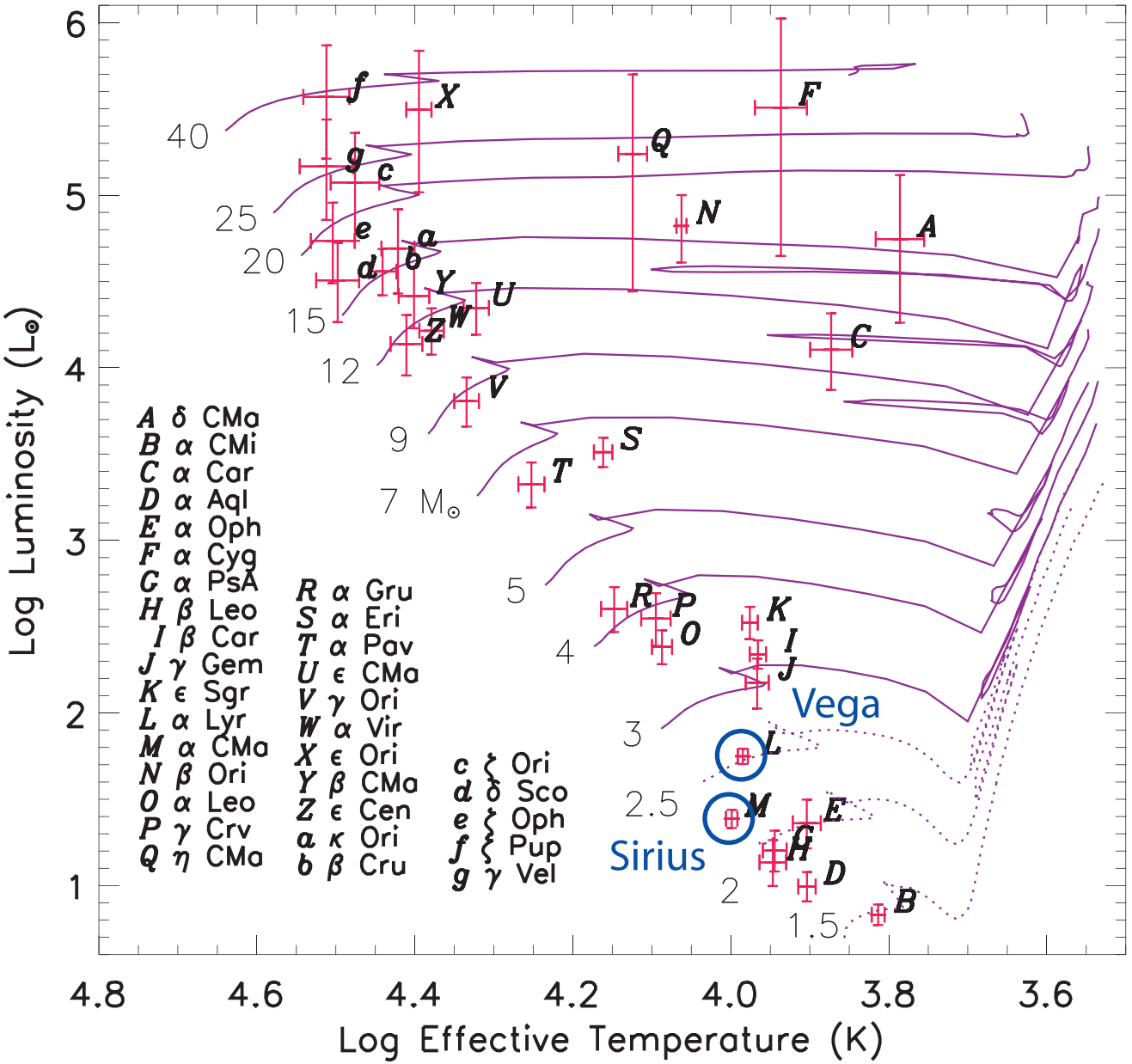

R. Hanbury Brown et al. (1967) measure angular diameters of Vega and Sirius with the Intensity Interferometer.

The homology relation

$$R \approx M^{0.715 \pm 0.035}$$

says that
R(Vega)/R(Sirius) should be ~ 1.12

Also: Vega is over luminous for its spectral type *and* has *weird* line profiles (Millward & Walter 1985; Gulliver et al. 1991).

Vega is a Pole-on Rapid Rotator (R. Gray 1985, 1988)

*Pole-on rapid rotators appear more luminous, have same color as slow rotators

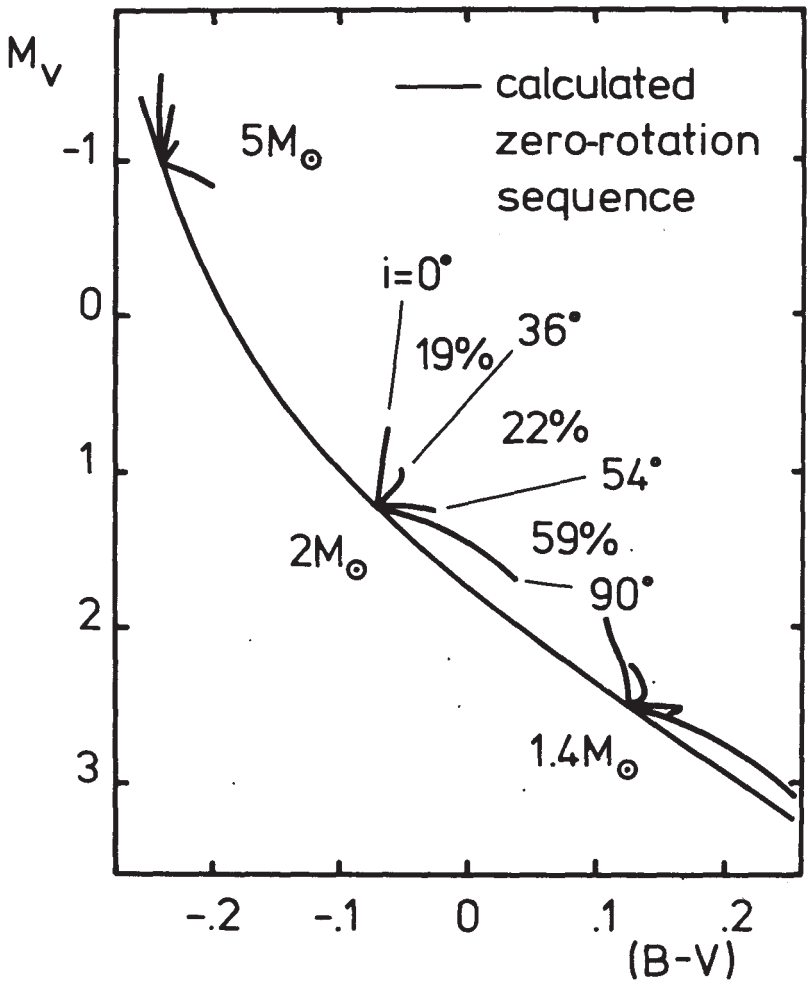

From Tassoul (1978) "Theory of Rotating Stars"
originally from Maeder & Peytremann (1970)

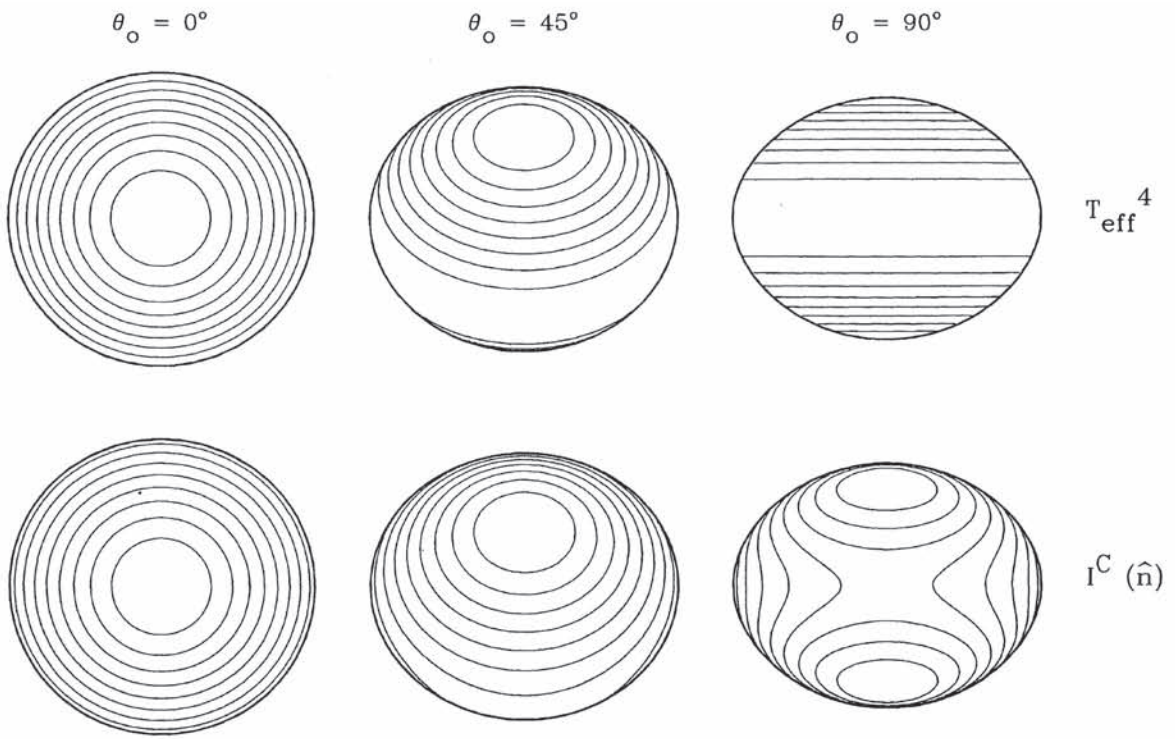

From Cranmer & Owocki (1995)

The Radiative Equilibrium of a Rotating System of Gaseous Masses.
By H. v. Zeipel, Assoc.R.A.S.

$$T_e^4 = \frac{\tilde{F}}{\pi\mu} = \frac{4}{ac}\tilde{F} = \frac{4}{aC}\frac{d\tilde{\Phi}}{dn_i}.$$

From von Zeipel (1924)

$T_{eff} \propto g^{1/4}$

Resolved Rapid Rotators from Interferometry

*Disk of Altair (A7 V) resolved as ellipsoid by the Palomar Testbed Interferometer (van Belle et al. 2001) Axial ratio: 1.140±0.029

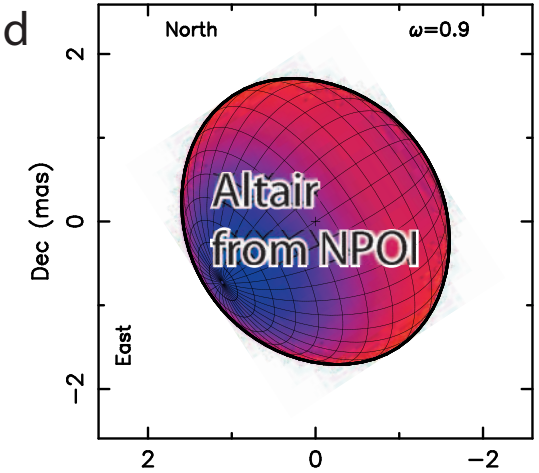

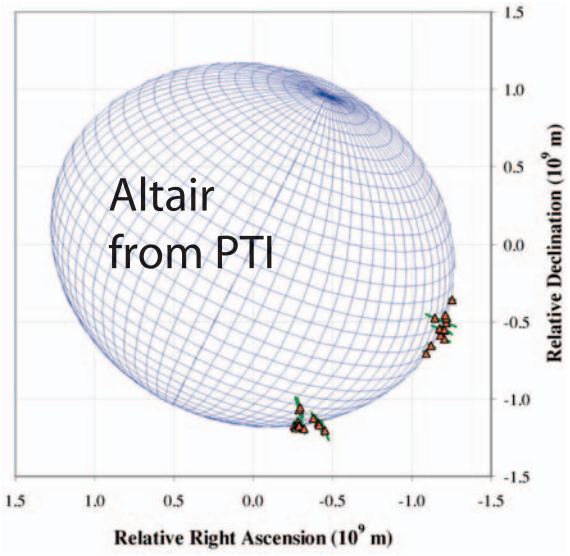

NPOI 3-telescope observations reveal 'hot spot' near pole (Ohishi et al. 2004)

Forthcoming Altair papers:
A. Domiciano de Souza et al. (VLTI+NPOI);
Peterson et al. 2006 (NPOI)

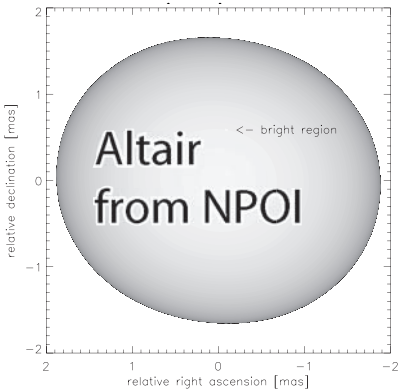

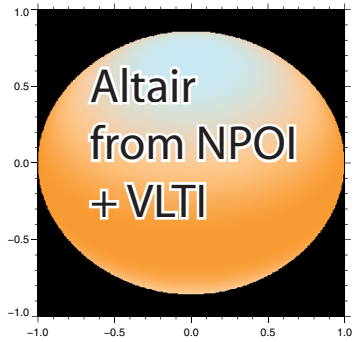

*Disk of Alderamin (A7 IV-V) resolved as an ellipsoid by CHARA (van Belle et al. 2006). Axial ratio: 1.298±0.051

*Disk of Regulus (B7 V) resolved as ellipsoid by CHARA (McAlister et al. 2005). Axial ratio: 1.32±0.02

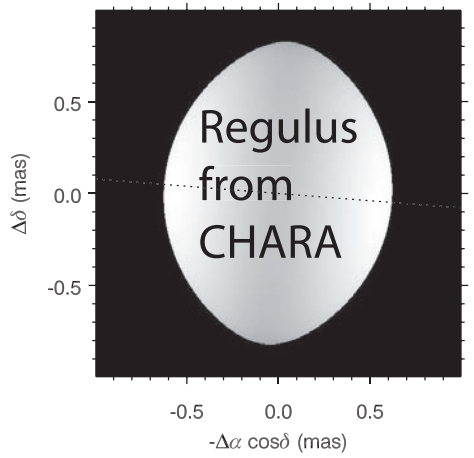

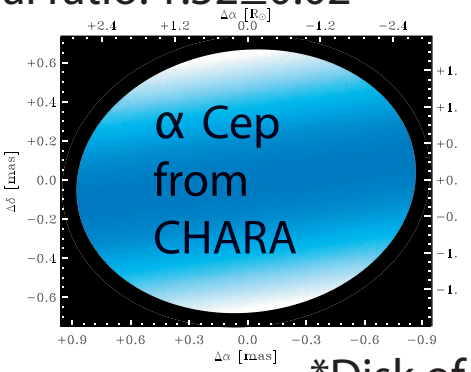

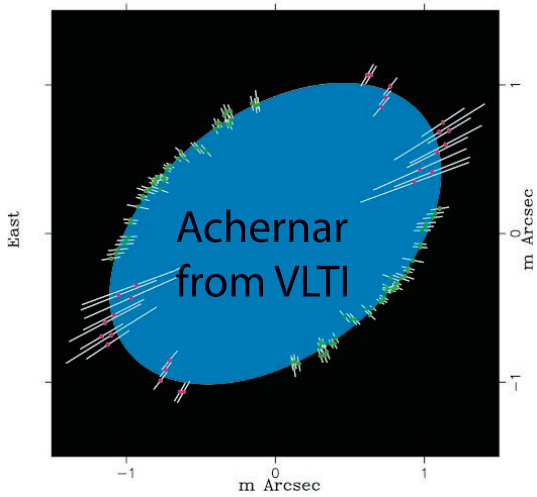

*Disk of Achernar (B3 Vpe) resolved as ellipsoid by VLTI (A. Domiciano de Souza et al. 2003). Axial ratio: 1.56±0.05

CHARA (Center for High Angular Resolution Astronomy) Array

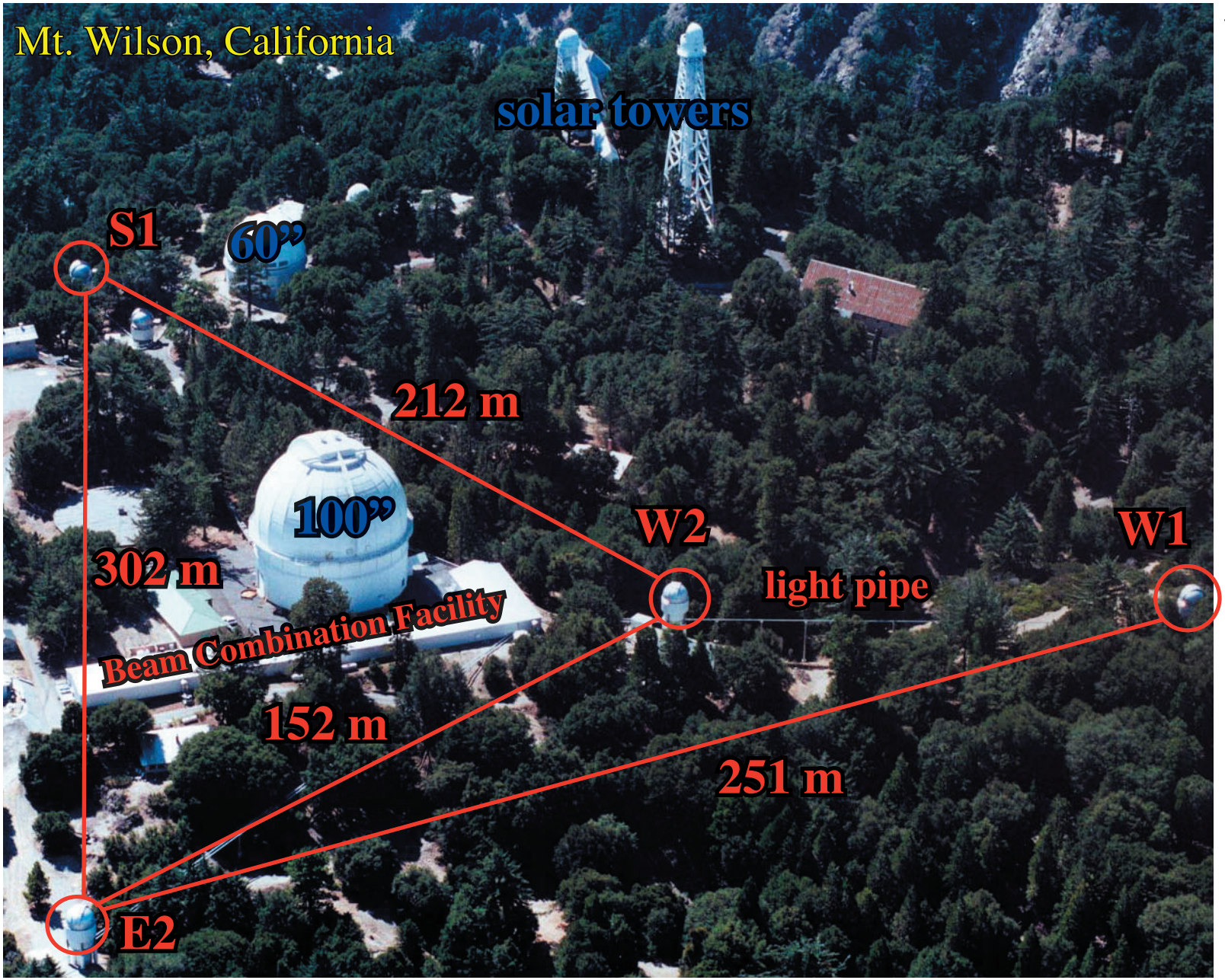

Vega Observations
May, June2005

K-band
$\lambda = 2.2\ \mu\mathrm{m}$

Fiber
Linked
Unit for
Optical
Recombination

beam combiner

(u,v) Coverage of Vega with the CHARA Array

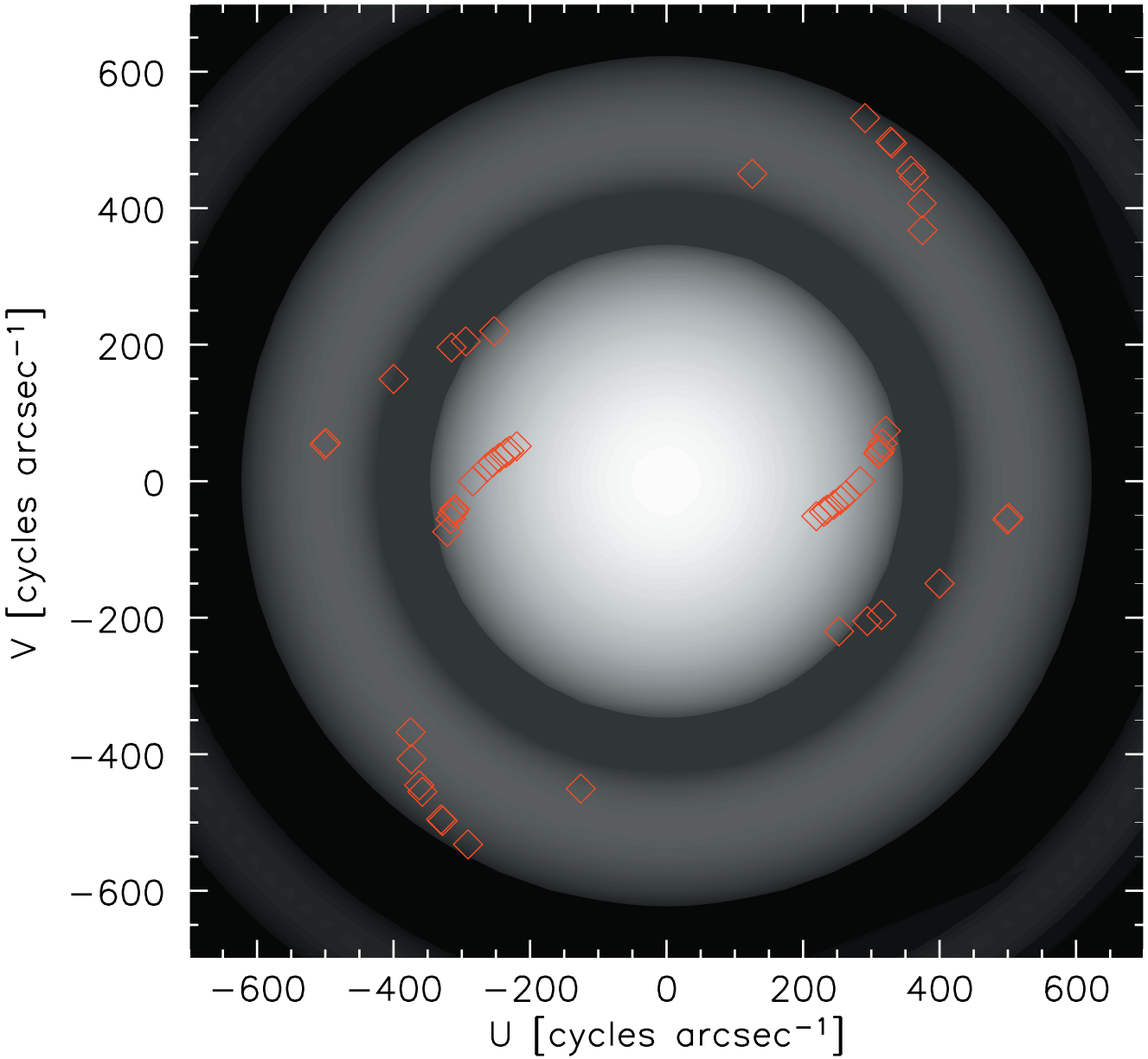

Fringes with CHARA/FLUOR!

Limb Darkening Basics

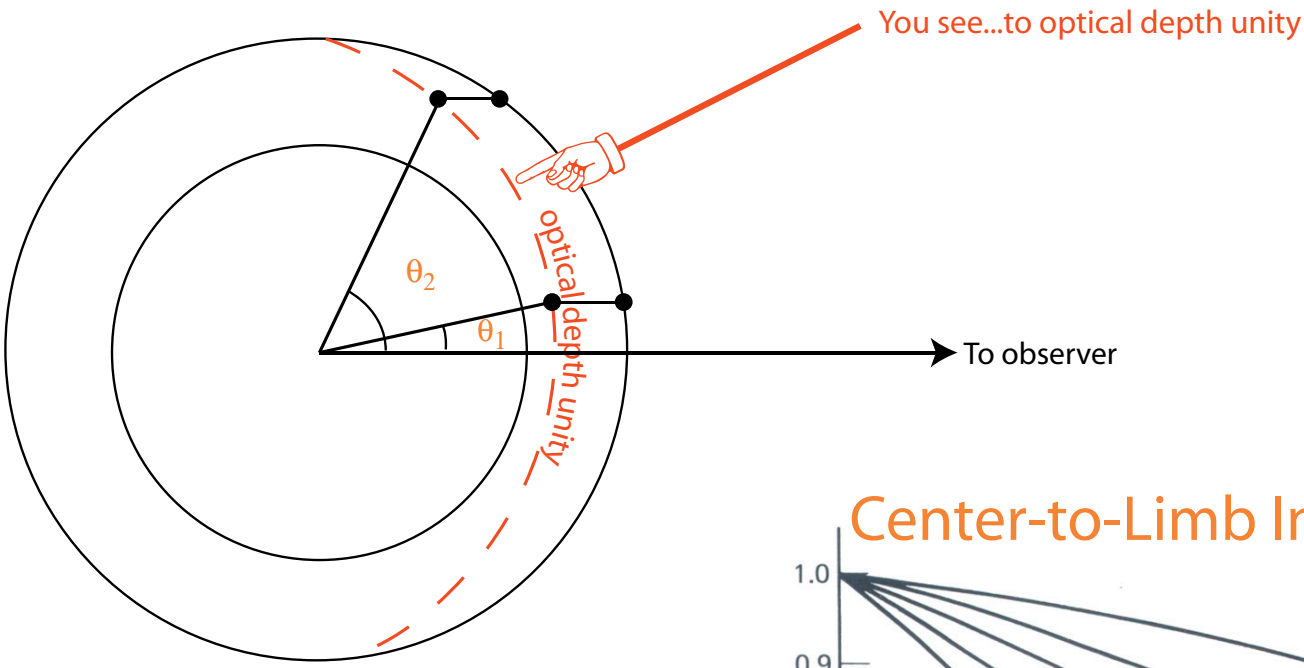

$$B_\lambda = 2\ ckT\ \lambda^{-4}$$

$$\frac{dB_\lambda}{dT} = \frac{2}{c} k\ \lambda^{-4}$$

Center-to-Limb Intensity Profile

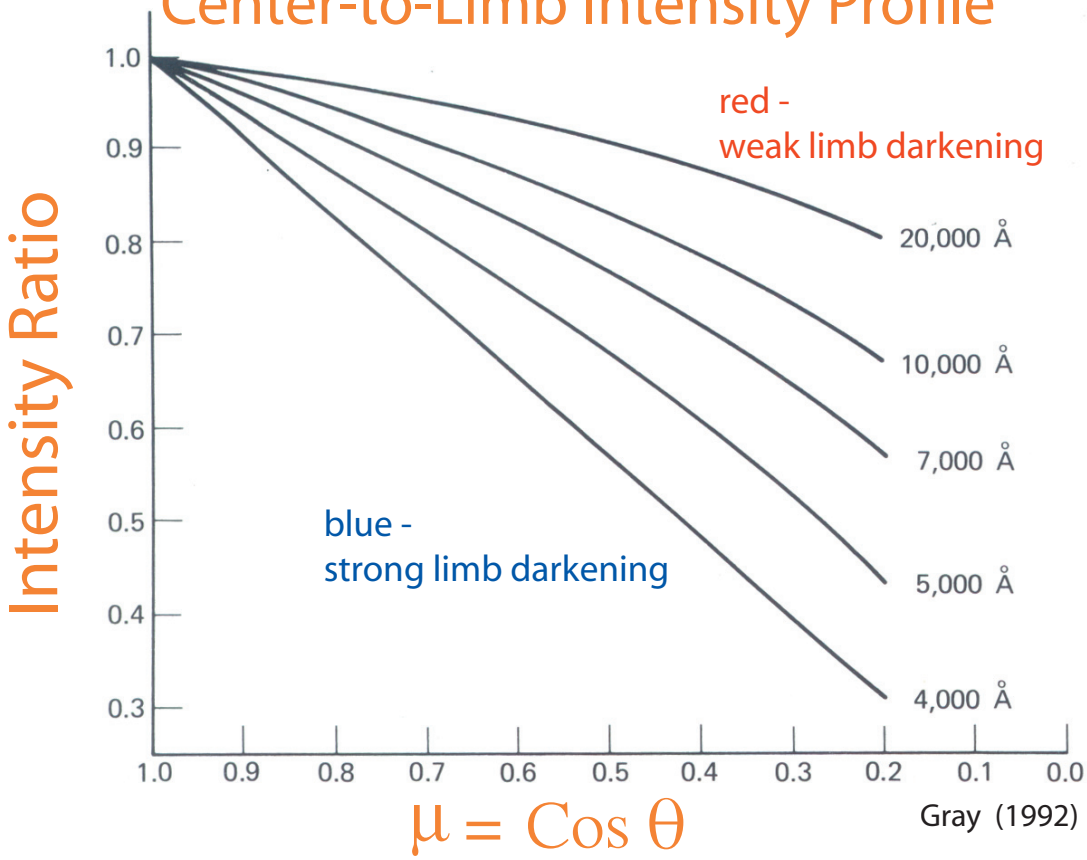

Gray (1992)

Observations and 1st Modeling

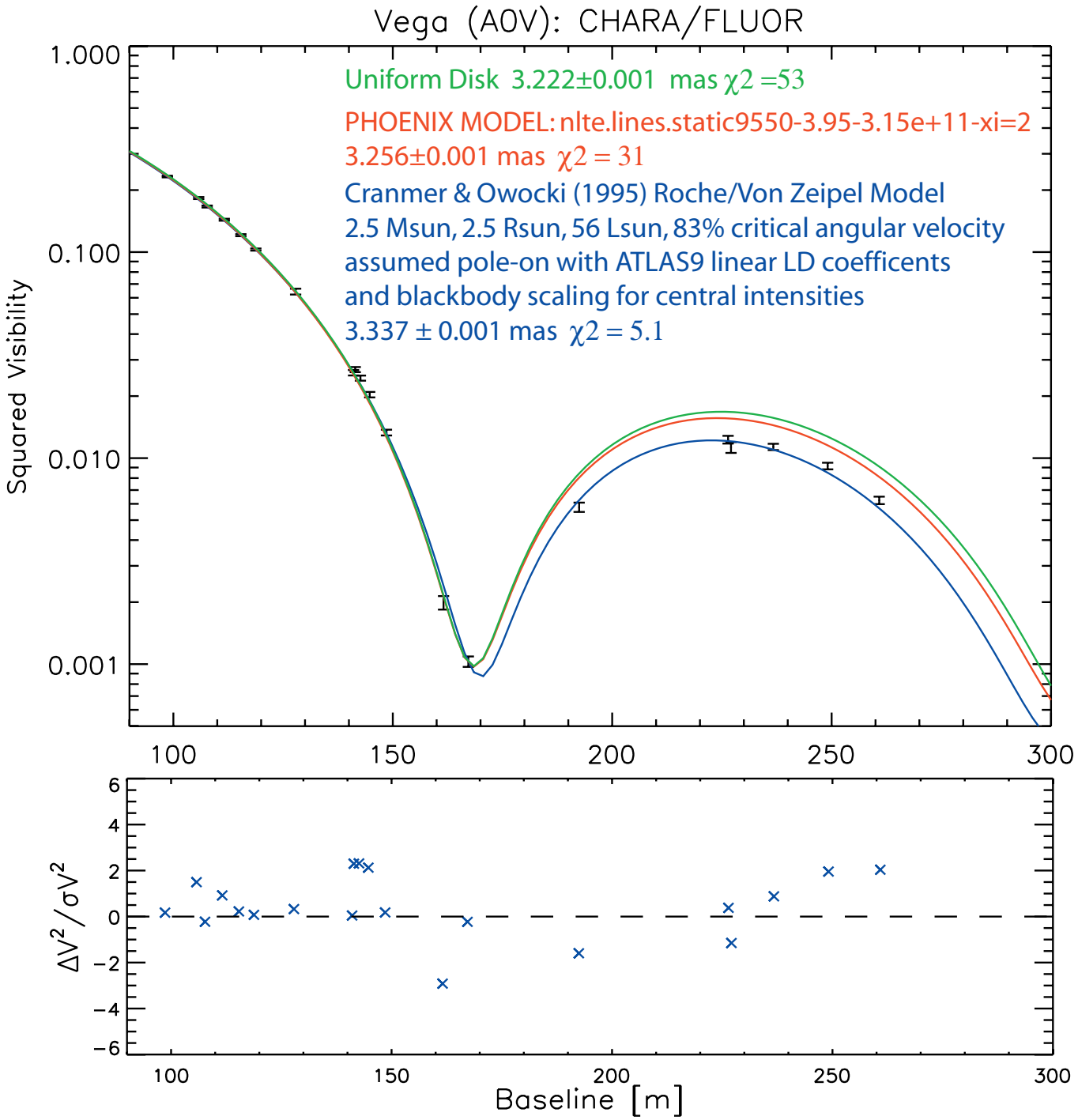

Parameterizing the Problem: 4 Variables and lots of equations!

$\omega \;\; \theta_{\rm equ} \;\; T_{\rm eff}^{\rm pole} \;\; g_{\rm pole}$

ω Fraction of the angular break-up speed

$\theta_{\rm equ}$ Equatorial Angular Diameter (physical AD of Vega viewed exactly pole-on)

$T_{\rm eff}^{\rm pole}$ Effective Temperature at the pole

$g_{\rm pole}$ Surface gravity at the pole

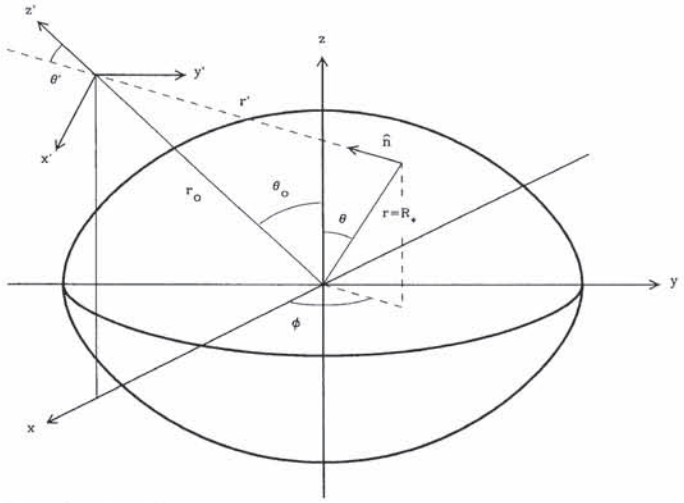

$$R_{\rm equ} = 107.48 \frac{\theta_{\rm equ}}{\pi_{\rm hip}}$$

$$R_{\rm pole} = \frac{\omega\, R_{\rm equ}}{3\,\cos\left[\dfrac{\pi + \cos^{-1}(\omega)}{3}\right]}$$

$$R(\vartheta) = 3\frac{R_{\rm pole}}{\omega \sin\vartheta}\cos\left[\frac{\pi + \cos^{-1}(\omega \sin\vartheta)}{3}\right]$$

$$g(\vartheta) = \left[g_r(\vartheta)^2 + g_\vartheta(\vartheta)^2\right]^{1/2}$$

$$g_r(\vartheta) = \frac{-GM}{R(\vartheta)^2} + R(\vartheta)(\Omega \sin\vartheta)^2$$

$$g_\vartheta(\vartheta) = R(\vartheta)\Omega^2 \sin\vartheta\cos\vartheta$$

$$M = \frac{g_{\rm pole}\, R_{\rm pole}^2}{G}$$

$$L = \frac{\sigma\Sigma(T_{\rm eff}^{\rm pole})^4}{g_{\rm pole}}$$

$$\frac{T_{\rm eff}(\vartheta)}{T_{\rm eff}^{\rm pole}} = \left(\frac{g(\vartheta)}{g_{\rm pole}}\right)^\beta$$

$$T_{\rm eff}(\vartheta) = \left[\frac{L}{\sigma\Sigma} g(\vartheta)\right]^\beta$$

$$\Omega = \omega\Omega_{\rm crit} = \omega\left[\frac{8}{27}\frac{GM}{R_{\rm pole}^3}\right]^{1/2}$$

$$V_{\rm equ} = R_{\rm equ}\,\Omega$$

$$i = \sin^{-1}\left[\frac{v \sin i}{V_{\rm equ}}\right]$$

$$\Sigma \approx 4\pi GM\Big[1.0 - 0.19696\,\omega^2 - 0.094292\,\omega^4 + 0.33812\,\omega^{\prime}$$

$$- 1.30660\,\omega^8 + 1.8286\,\omega^{10} - 0.92714\,\omega^{12}\Big]$$

Accurate Synthetic Visibilities with High Dynamic Range

2-D Fourier Transform

$$V_\lambda^2(u,v) = \left[\int_{-\infty}^{\infty}\int_{-\infty}^{\infty} S_\lambda I_\lambda(x,y) e^{i2\pi(u\,x+v\,y)}\,\mathrm{d}x\,\mathrm{d}y\right]^2$$

Numerical "Cubature"
N=512

$$V^2(u_k,v_k) \approx \left[\sum_{i=1}^{N} A_i \sum_{j=1}^{N} A_j S_k I_k(x_i,y_j)\cos(2\pi(u_k x_i + v_k y_j))\right]^2 + \left[\sum_{i=1}^{N} A_i \sum_{j=1}^{N} A_j S_k I_k(x_i,y_j)\sin(2\pi(u_k x_i + v_k y_j))\right]^2$$

CPU time for 26 (u,v) points is ~6x faster than a 4096x4096 FFT

The 2-D Modeling Problem

Intensity Map: Vega (pole-on)

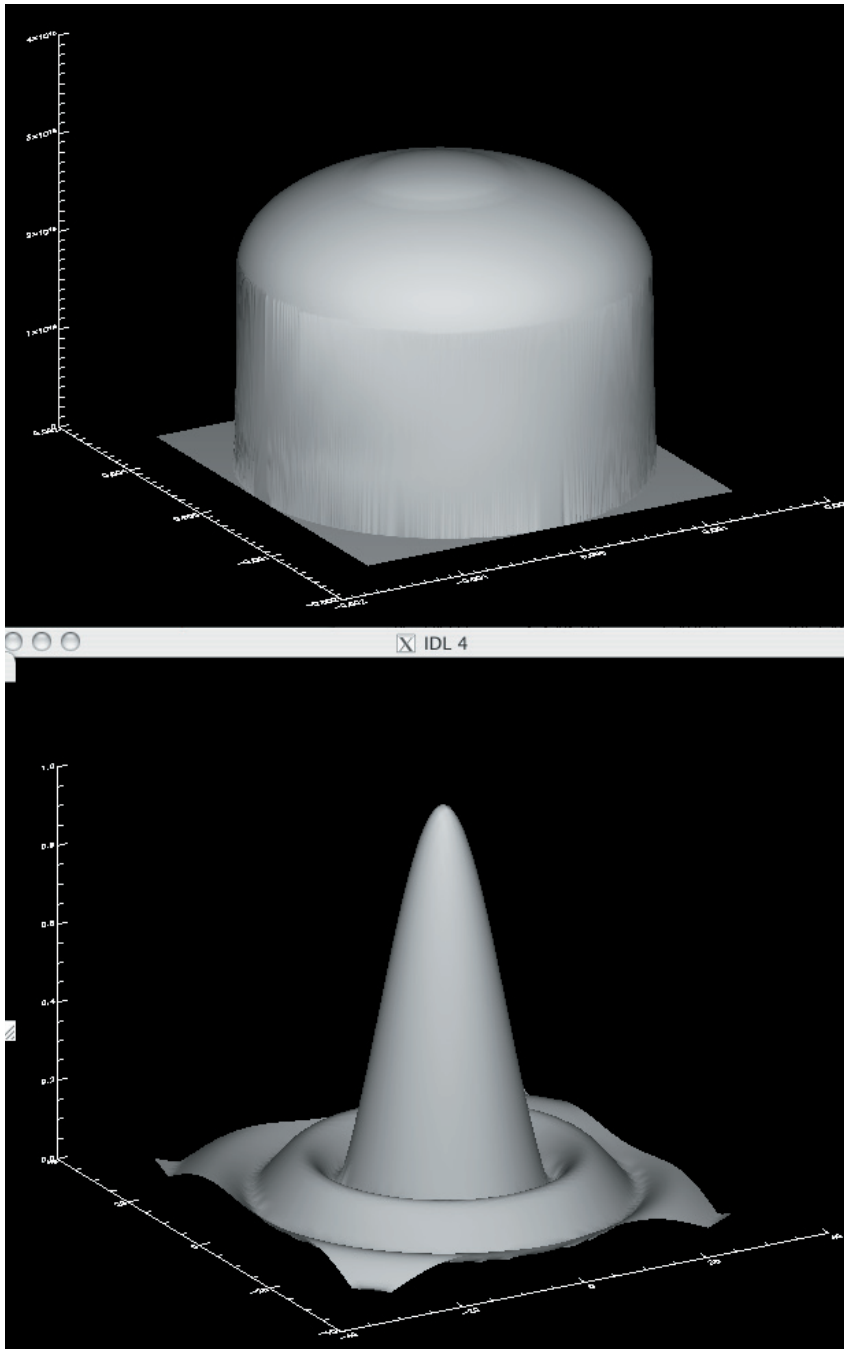

Fast Fourier Transform—»

Intensity Map: Vega (equator-on)

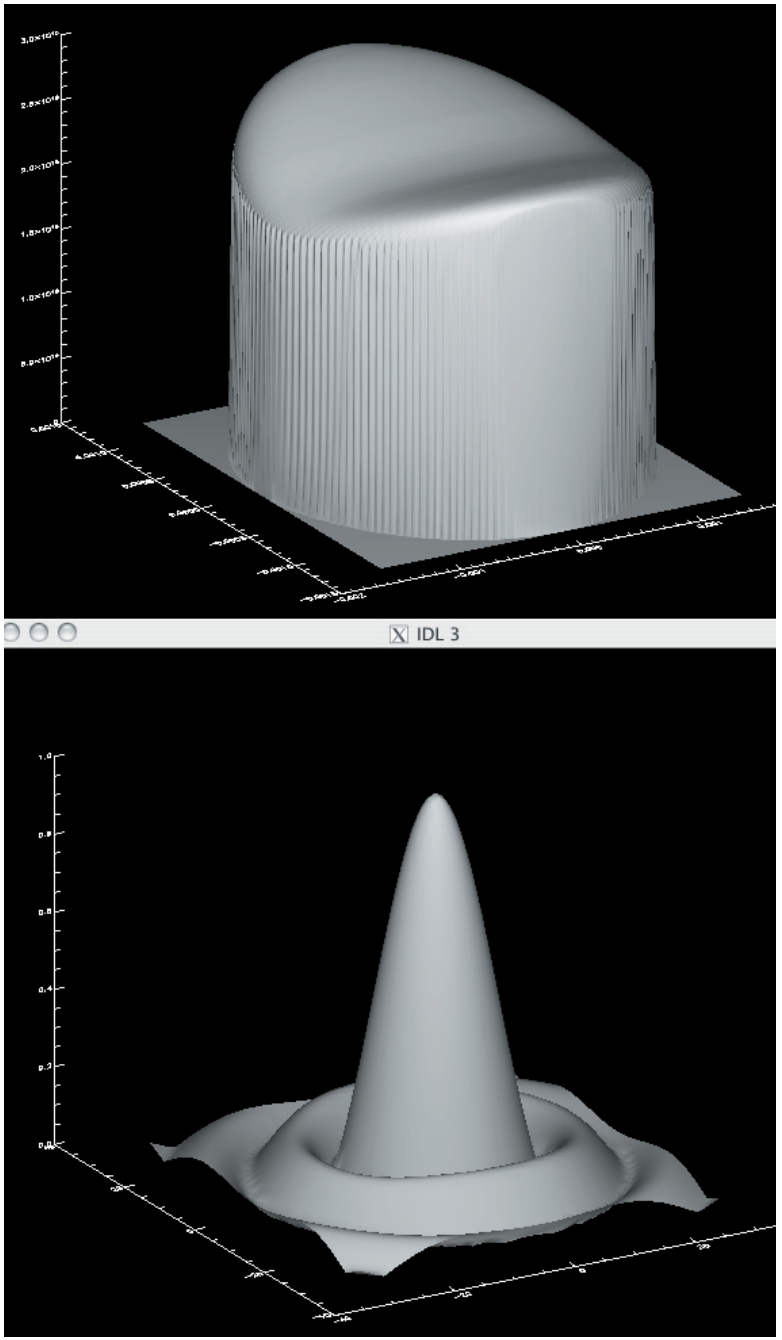

Rotating Model Fit to the CHARA/FLUOR Visibility Data

Model Input Parameters

T_{eff} (pole)	= 10250 K B9
T_{eff} (equator)	= 7700 K A9
Log(g) (pole)	= 4.10
ω (angular break-up fraction)	= 0.93
$\theta_{equator}$	= 3.34 mas

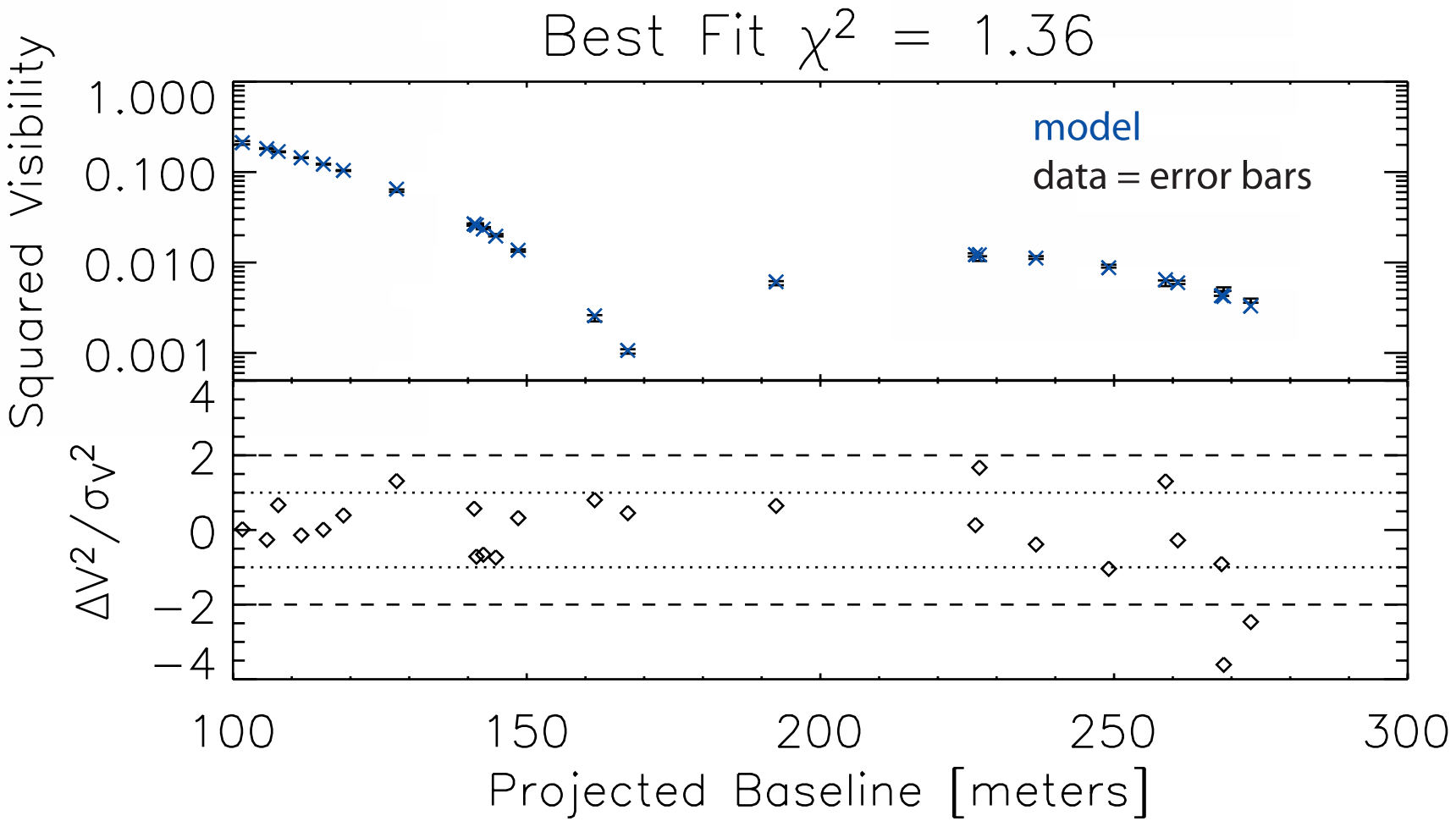

Searching the 5-D Hypercube! Preliminary Fit Results for Vega

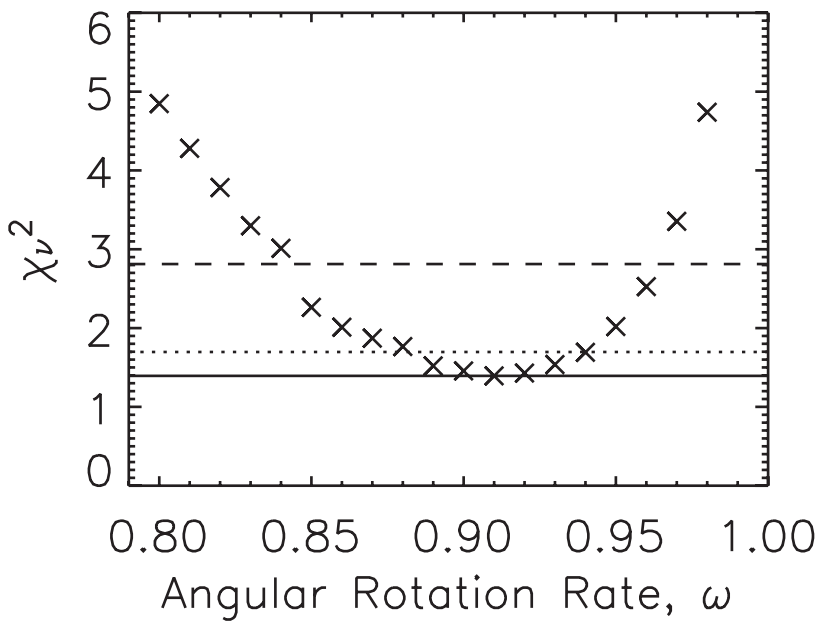

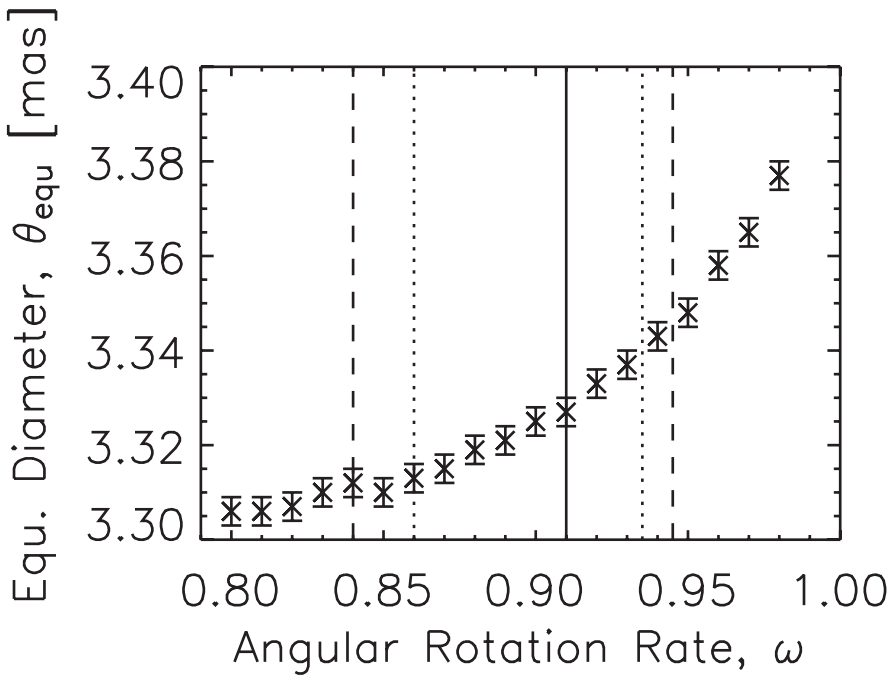

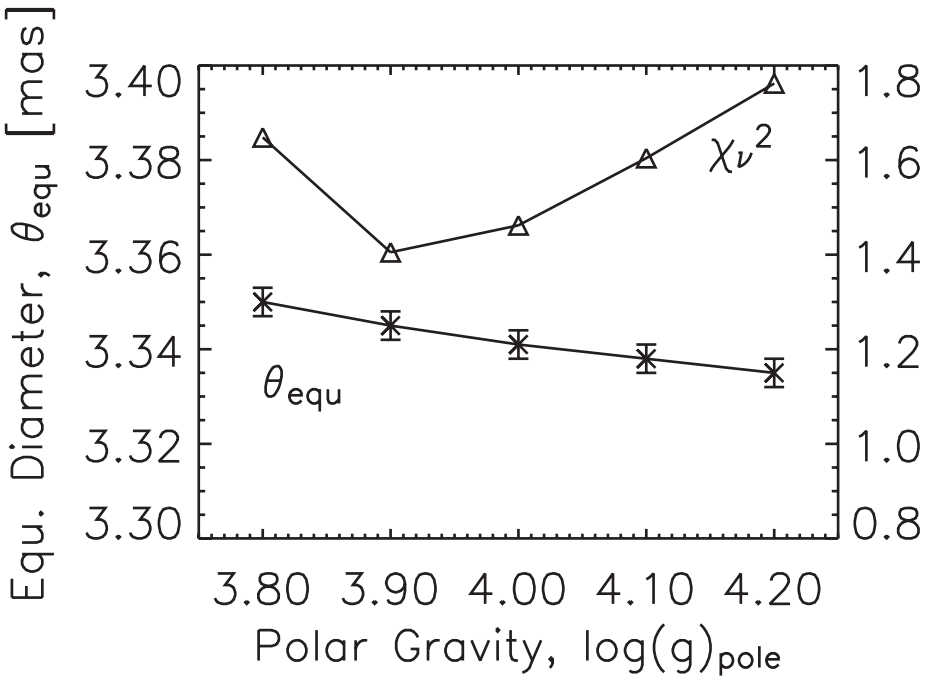

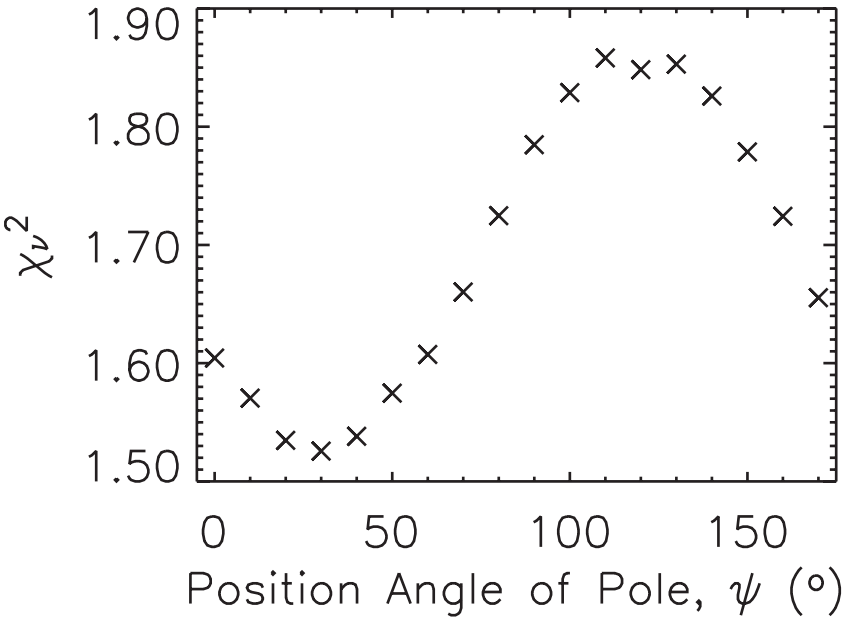

Spectral Energy Distribution Comparison

$$F_\lambda = \int_0^{\pi} \int_0^{2\pi} -\frac{g(\vartheta)}{g_r(\vartheta)} I_\lambda(R, \vartheta, \varphi) R(\vartheta)^2 \sin\vartheta \mu(\vartheta, \varphi, i)\, \mathrm{d}\varphi\, \mathrm{d}\vartheta$$

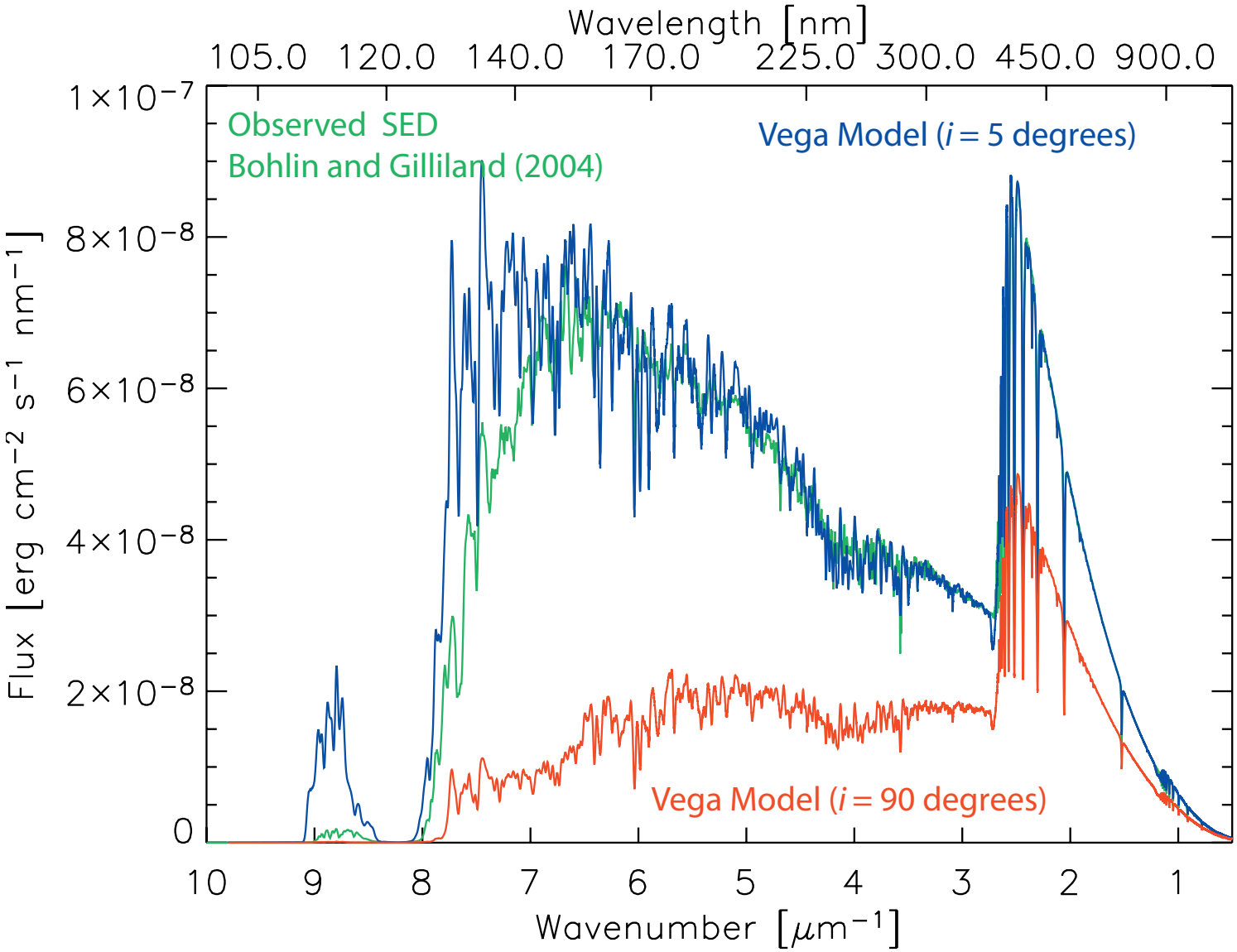

T_{eff} (Pole) = 10250 K
Log(g) (Pole) = 3.95
ω = 0.92
$\theta_{equator}$ = 3.40 milliarcsecond

Vega's disk sees a ~7700 K SED

IRAS

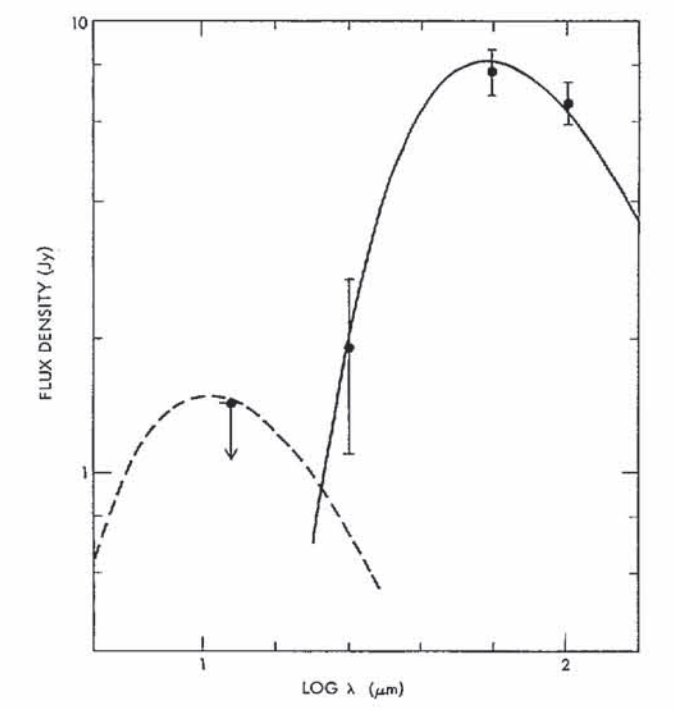

Aumann et al. (1984)

Spitzer

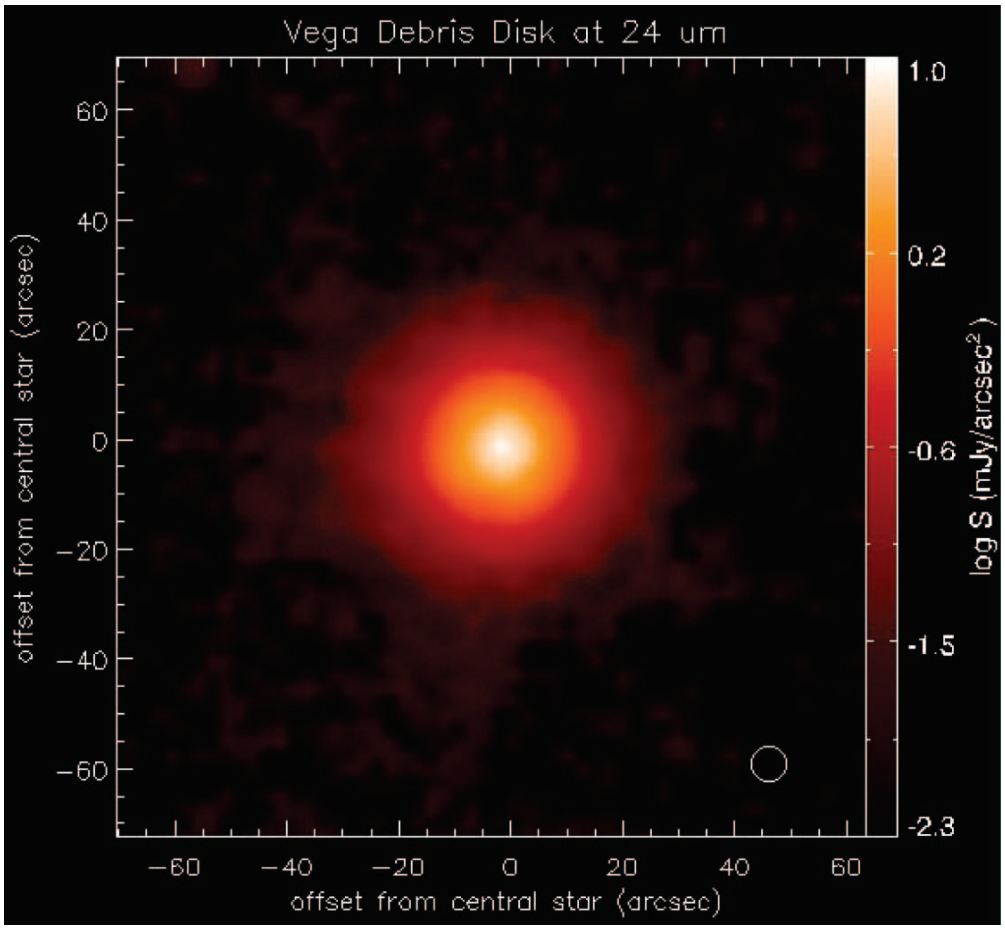

Su et al. (2005)

Procyon

Procyon: The Visual Binary (P = 40.82 yr)

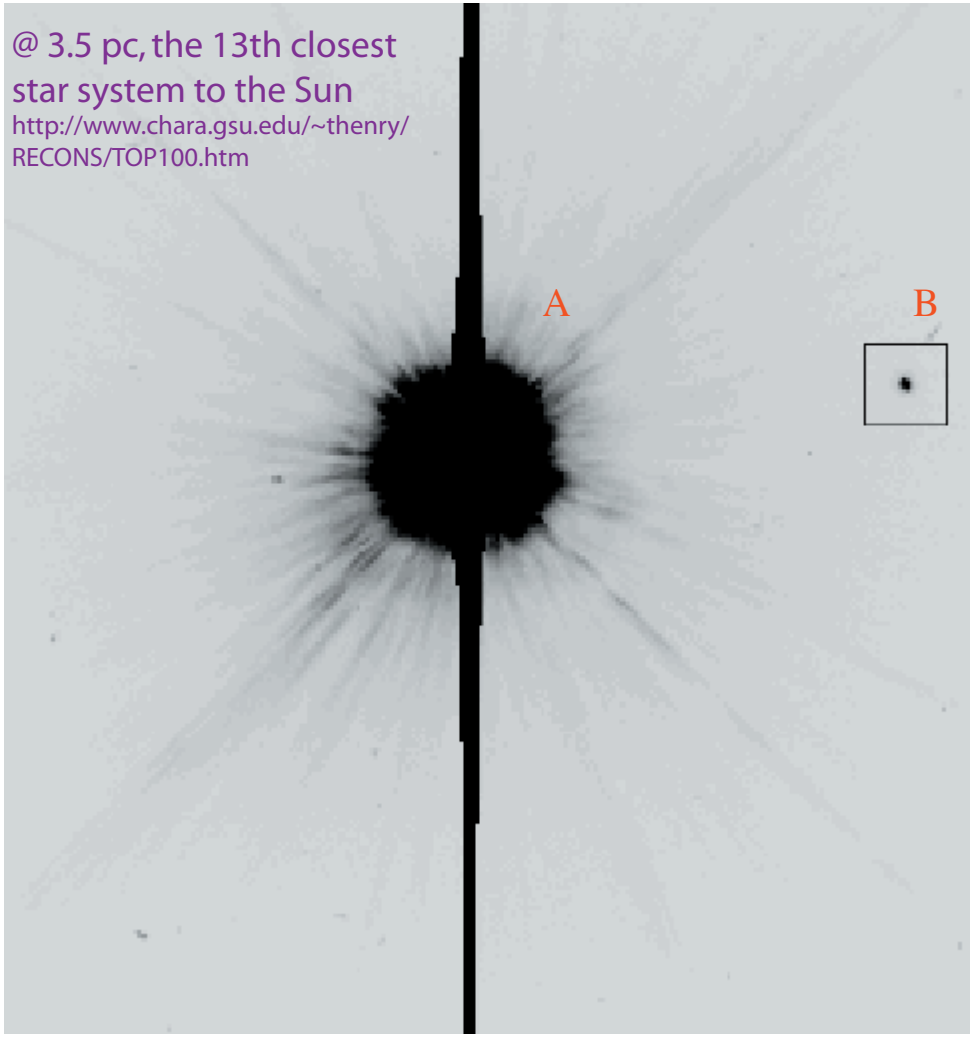

Girard et al (2000) ApJ 119, 2428

HST/WFPC2 PC image (160 s)
F218W filter

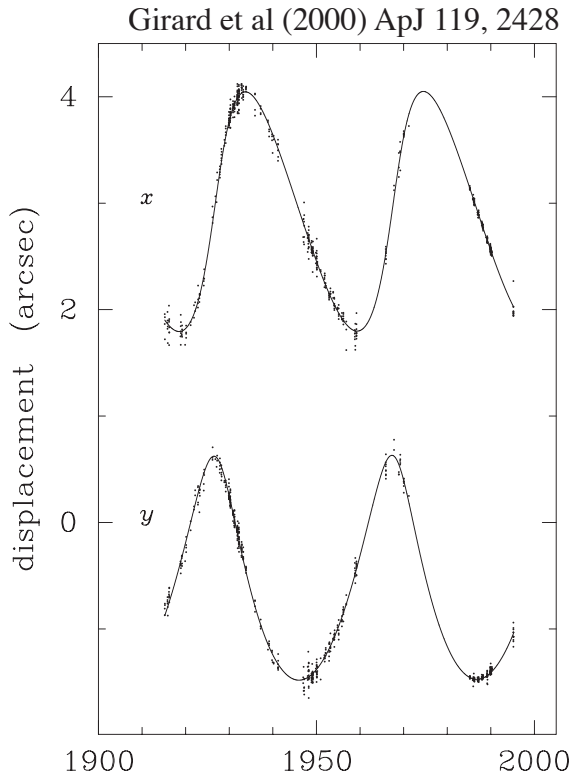

$Mass_A = 1.497 \pm 0.037\ M_\odot$
$Mass_B = 0.602 \pm 0.015\ M_\odot$

Procyon A (F5 IV): Fundamental Parameters

Angular diameter = 5.45 ± 0.05 mas (Kervella et al. 2003)
Parallax = 285.93 ± 0.88 mas (Hipparcos: Perryman et al.)
Radius = 2.05 ± 0.02 $R_\odot$
Log(g) = 3.95 ± 0.02 cgs
Bolometric flux = 17.8 ± 0.9 x 10^{-9} W m^{-2}
Effective Temperature = 6516 ± 87 K

Early Model Limb Darkening Models

1906 - K. Schwarzschild
Derived a center-to-limb profile for the Sun with a radiative equilibrium temperature structure. He showed this to be consistent with observations, ruling out an adiabatic equilibrium temperature structure.

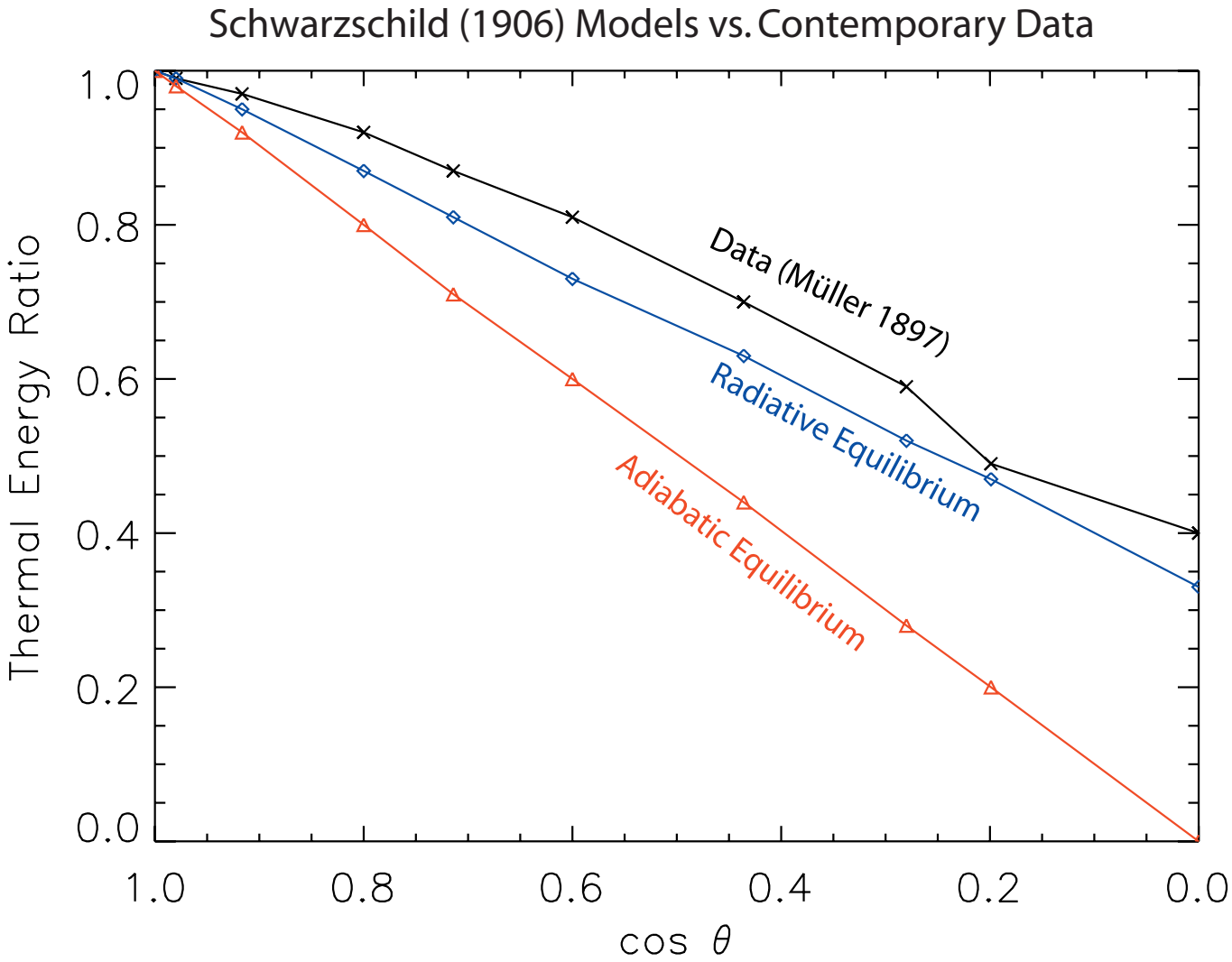

Assumptions: mass absorption coefficent is both wavelength and depth independent. Angular-dependent intensity is replaced by its mean.

Adapted from K. Schwarzschild (1906) "Über das Gleichgewicht der Sonnenatmosphäre"
Nachrichten von der Königlichen Gesellschaft der Wissenschaften zu Göttingen. Math.-phys. Kalsse, 295, 41
Translation in D. H. Menzel, Ed., *Selected Papers on the Transfer of Radiation* (1966) NY: Dover

Solar Limb Darkening and the Overshooting Approximation

Castelli, Gratton & Kurucz (1997) A&A 318, 841

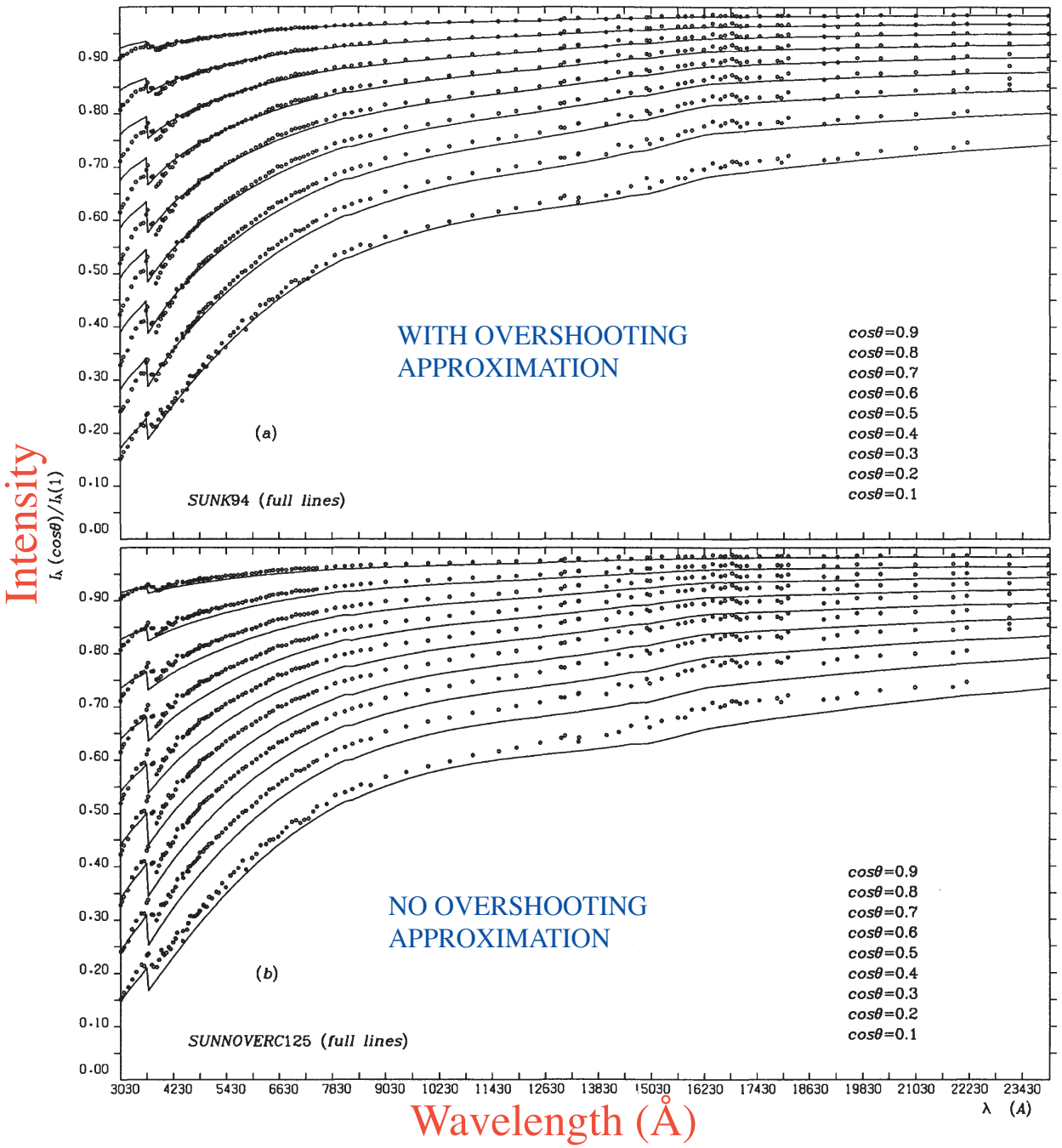

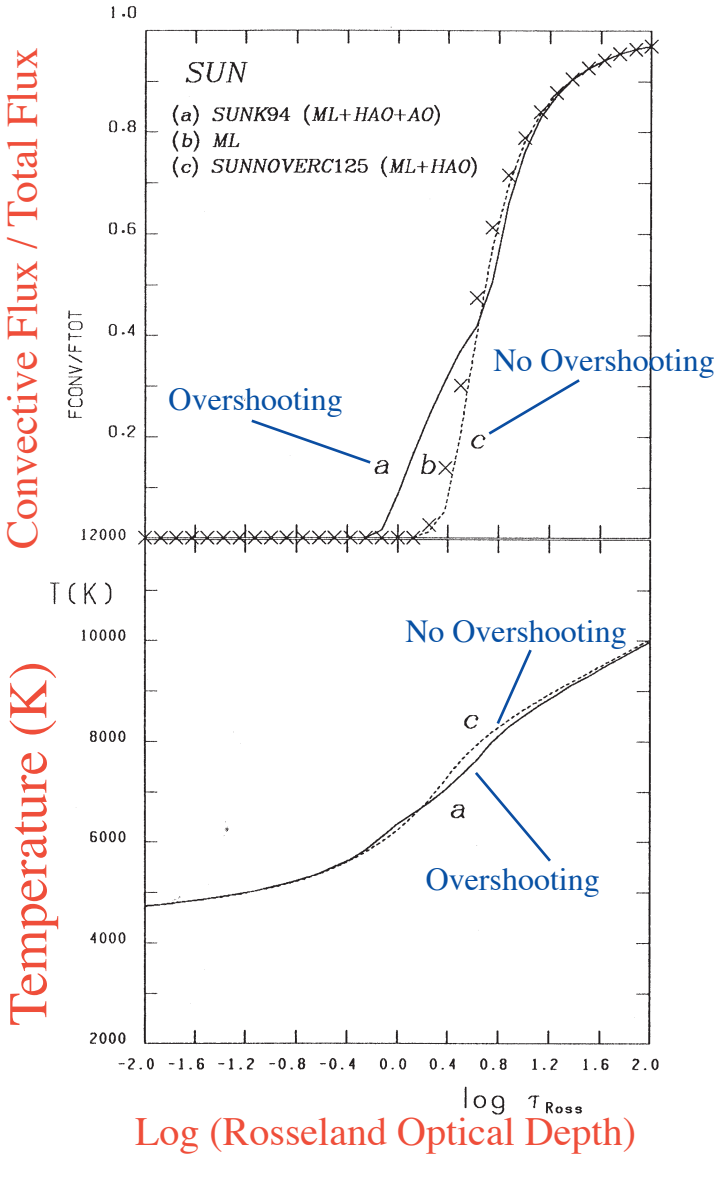

A&A 417, 751–768 (2004)
DOI: 10.1051/0004-6361:20034328

Astronomy & Astrophysics

Asplund et al. (2004) A&A 417, 751

Line formation in solar granulation

IV. [O I], O I and OH lines and the photospheric O abundance

M. Asplund[1], N. Grevesse[2,3], A. J. Sauval[4], C. Allende Prieto[5], and D. Kiselman[6]

[1] Research School of Astronomy and Astrophysics, Mt. Stromlo Observatory, Cotter Rd., Weston, ACT 2611, Australia
[2] Centre Spatial de Liège, Université de Liège, avenue Pré Aily, 4031 Angleur-Liège, Belgium
[3] Institut d'Astrophysique et de Géophysique, Université de Liège, Allée du 6 août, 17, B5C, 4000 Liège, Belgium
[4] Observatoire Royal de Belgique, avenue circulaire, 3, 1180 Bruxelles, Belgium
[5] McDonald Observatory and Department of Astronomy, University of Texas, Austin, TX 78712-1083, USA
[6] The Institute for Solar Physics of the Royal Swedish Academy of Sciences, AlbaNova University Centre, 106 91 Stockholm, Sweden

Received 17 September 2003 / Accepted 2 December 2003

Abstract. The solar photospheric oxygen abundance has been determined from [O I], O I, OH vibration-rotation and OH pure rotation lines by means of a realistic time-dependent, 3D, hydrodynamical model of the solar atmosphere. In the case of the O I lines, 3D non-LTE calculations have been performed, revealing significant departures from LTE as a result of photon losses in the lines. We derive a solar oxygen abundance of $\log \epsilon_O = 8.66 \pm 0.05$. All oxygen diagnostics yield highly consistent abundances, in sharp contrast with the results of classical 1D model atmospheres. This low value is in good agreement with measurements of the local interstellar medium and nearby B stars. This low abundance is also supported by the excellent correspondence between lines of very different line formation sensitivities, and between the observed and predicted line shapes and center-to-limb variations. Together with the corresponding down-ward revisions of the solar carbon, nitrogen and neon abundances, the resulting significant decrease in solar metal mass fraction to $Z = 0.0126$ can, however, potentially spoil the impressive agreement between predicted and observed sound speed in the solar interior determined from helioseismology.

Key words. convection – line: formation – Sun: abundances – Sun: granulation – Sun: photosphere

Recent 3-D radiative transfer models have reduced the solar oxygen abundance by nearly a factor of 2!

We derive a solar oxygen abundance of $\log \epsilon_O = 8.66 \pm 0.05$.

1. Introduction

Oxygen is the most abundant element in the Universe with a non-Big Bang nucleosynthesis origin. As a consequence, oxygen plays a central role in many different fields of astrophysics ranging from supernova physics and galaxy evolution to dating stars and production of the light elements through cosmic ray spallation. Yet it appears that in many crucial objects for which accurate knowledge of the oxygen abundances is necessary the oxygen content is hotly debated. Recent disputes revolve around the overabundance of oxygen in metal-poor halo stars (see Asplund & García Pérez 2001; Nissen et al. 2002, and references therein), the Galactic radial abundance gradient (Rolleston et al. 2000; Cunha & Daflon 2003), and, astonishingly, the solar oxygen abundance. Partly these disagreements stem from differences in the adopted input data (e.g. gf-values, effective temperatures $T_{\rm eff}$, surface gravities $\log g$) but more importantly they reflect the choice of spectral lines to derive the abundances using classical 1D stellar model atmospheres. In particular in the solar case, the freedom of parameters to obtain consistency is very restricted yet the discrepancy is present in full.

Until recently the commonly adopted solar oxygen abundance was $\log \epsilon_O = 8.93 \pm 0.04$[1] (Anders & Grevesse 1989). This historically high abundance was suggested by analyses of the forbidden [O I] 630.0 nm line (Lambert 1978) as well as OH vibration-rotation and pure rotation lines in the infrared (Grevesse et al. 1984; Sauval et al. 1984) using the 1D hydrostatic Holweger-Müller (1974) semi-empirical model of the solar atmosphere and LTE line formation. On the other hand, a much lower abundance is indicated by the permitted high-excitation O I lines, most noteworthy the IR triplet at 777 nm, when employing the same model atmosphere with non-LTE line formation. This discrepancy of about 0.2 dex between different abundance indicators have often been blamed on over-estimated departures from local thermodynamic

Until recently the commonly adopted solar oxygen abundance was $\log \epsilon_O = 8.93 \pm 0.04^1$ (Anders & Grevesse 1989).

Send offprint requests to: M. Asplund,
e-mail: martin@mso.anu.edu.au

[1] On the customary abundance scale defined as $\epsilon(\mathrm{X}) = 10^{12} \times N(\mathrm{X})/N(\mathrm{H})$.

3-D Hydrodynamical Simulations of Procyon

Allende Prieto et al (2002) ApJ 567, 544

500 K Teff
Surface R.M.S.

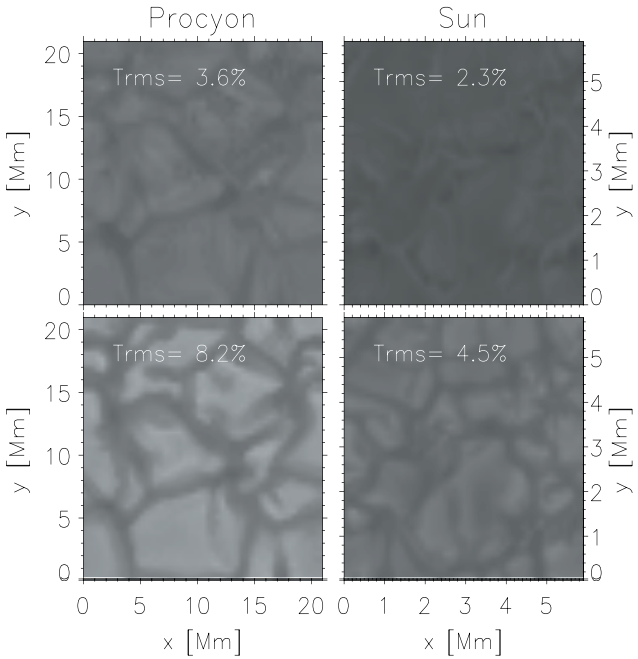

$\tau = 0.3$

$\tau = 1.0$

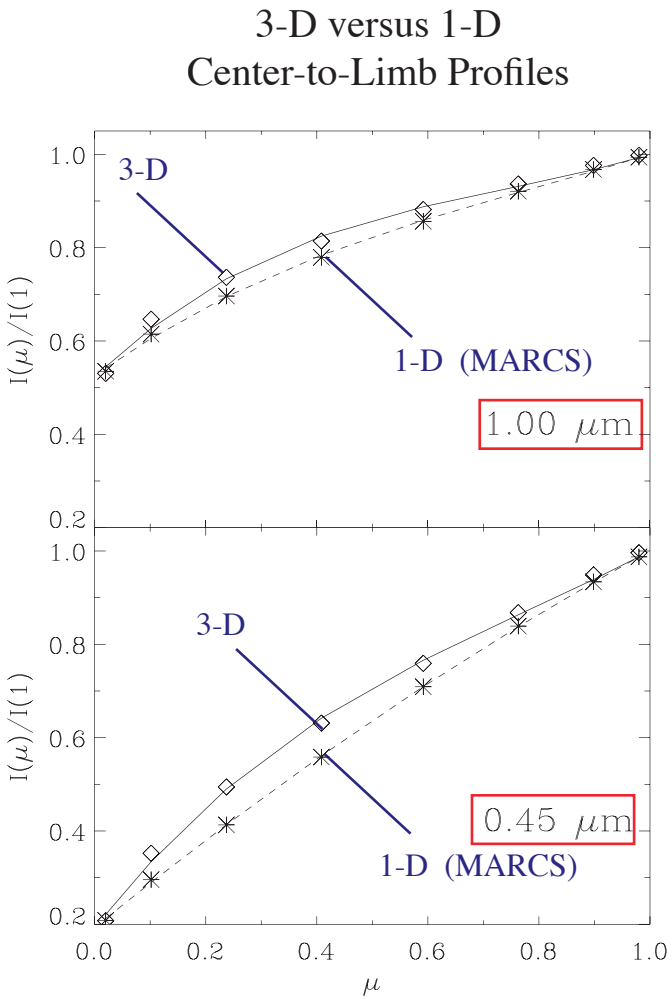

FIG. 19.—Limb darkening for the three-dimensional (*rhombi*) and one-dimensional (*asterisks*) models. Third-order polynomials have been fitted by regular least-squares fits to the data.

Prediction:
1.6 %
angular size
difference
between
1 micron
and
450 nm

Procyon Data from the Mark III and VLTI/VINCI

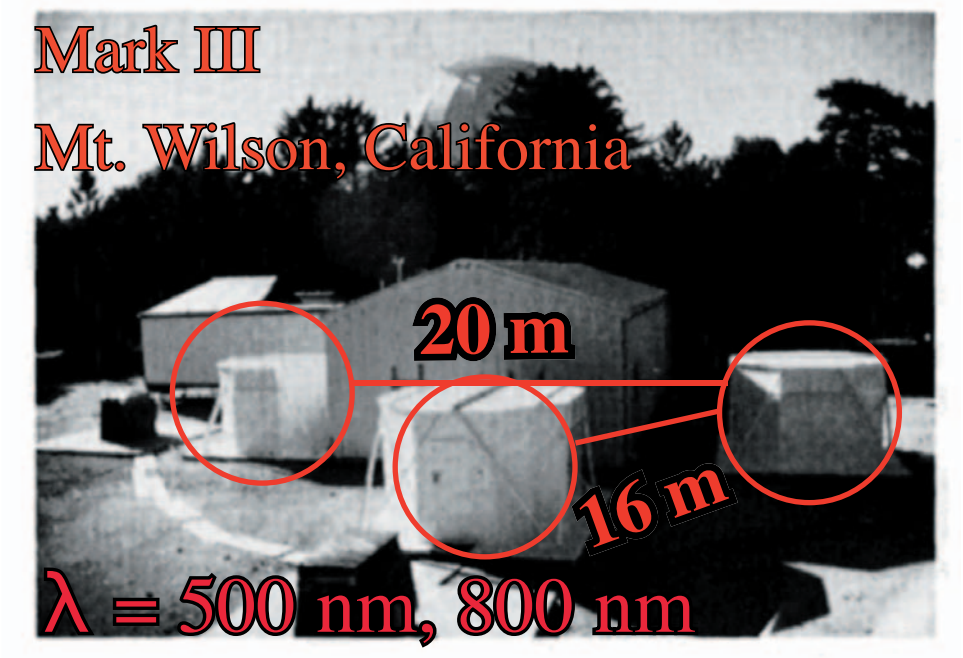

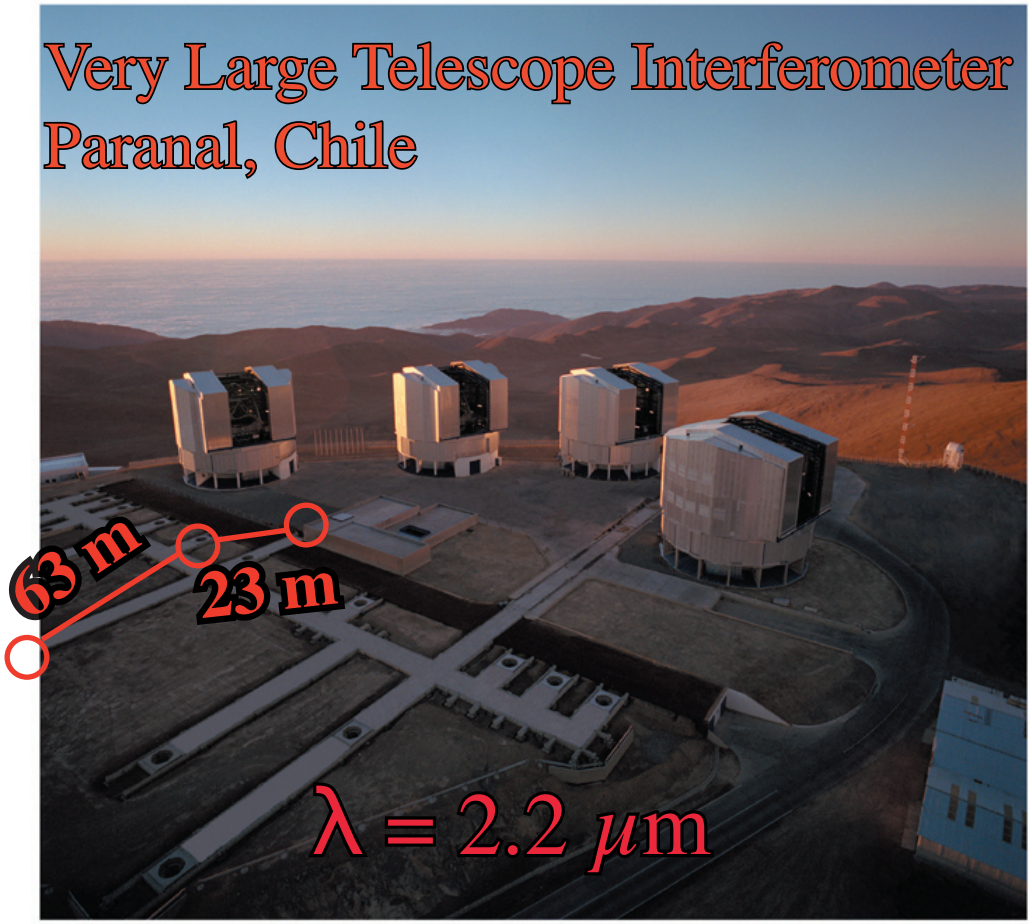

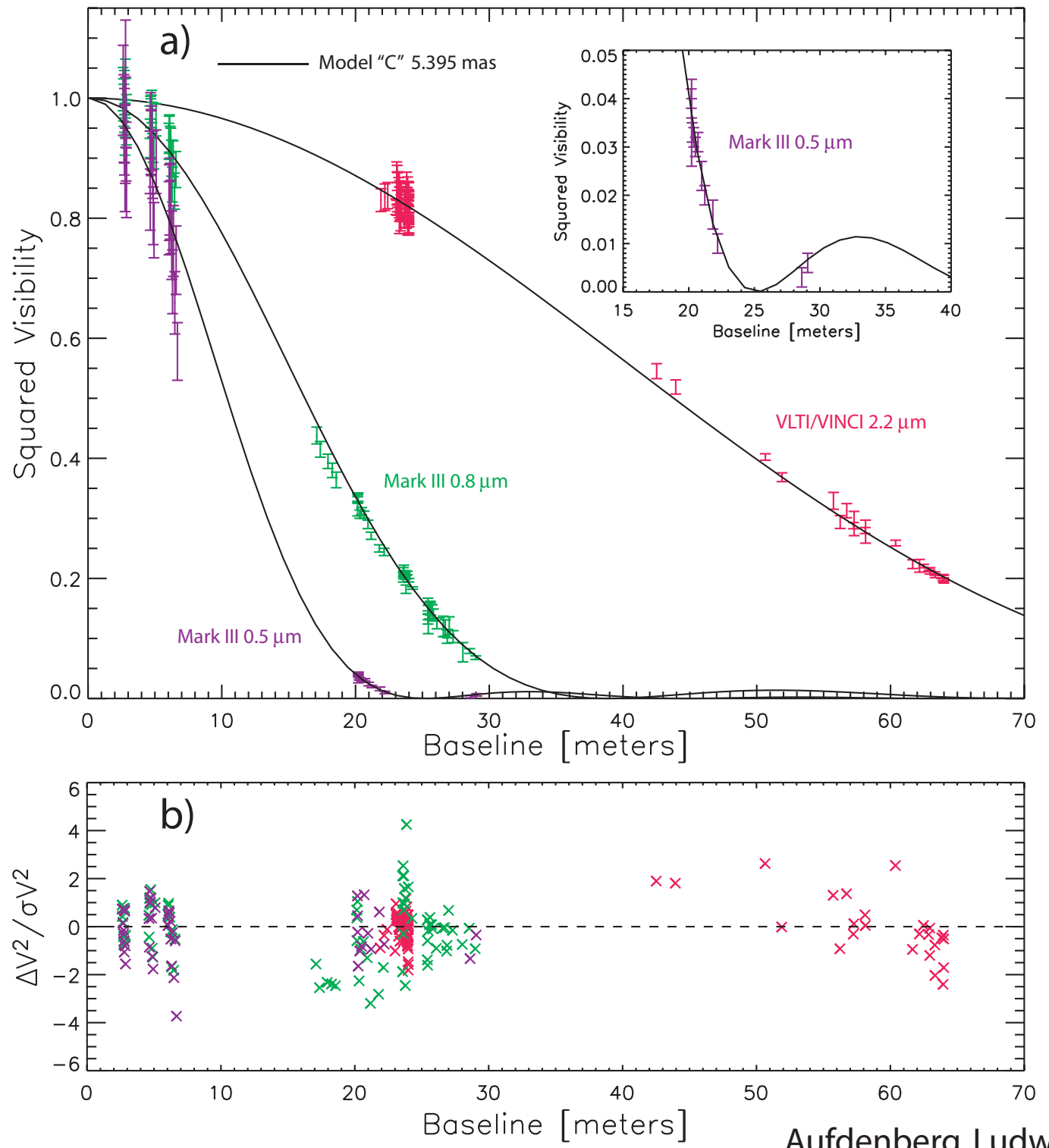

3-D CO^{5}BOLD Model Atmosphere synthetic visibilities

vs.

Mark III 500 nm, 800nm VLTI/VINCI K-band visibility data

Aufdenberg, Ludwig, & Kervella (2005) ApJ, 633, 424

Angular Diameters from 1-D & 3-D Model Fits

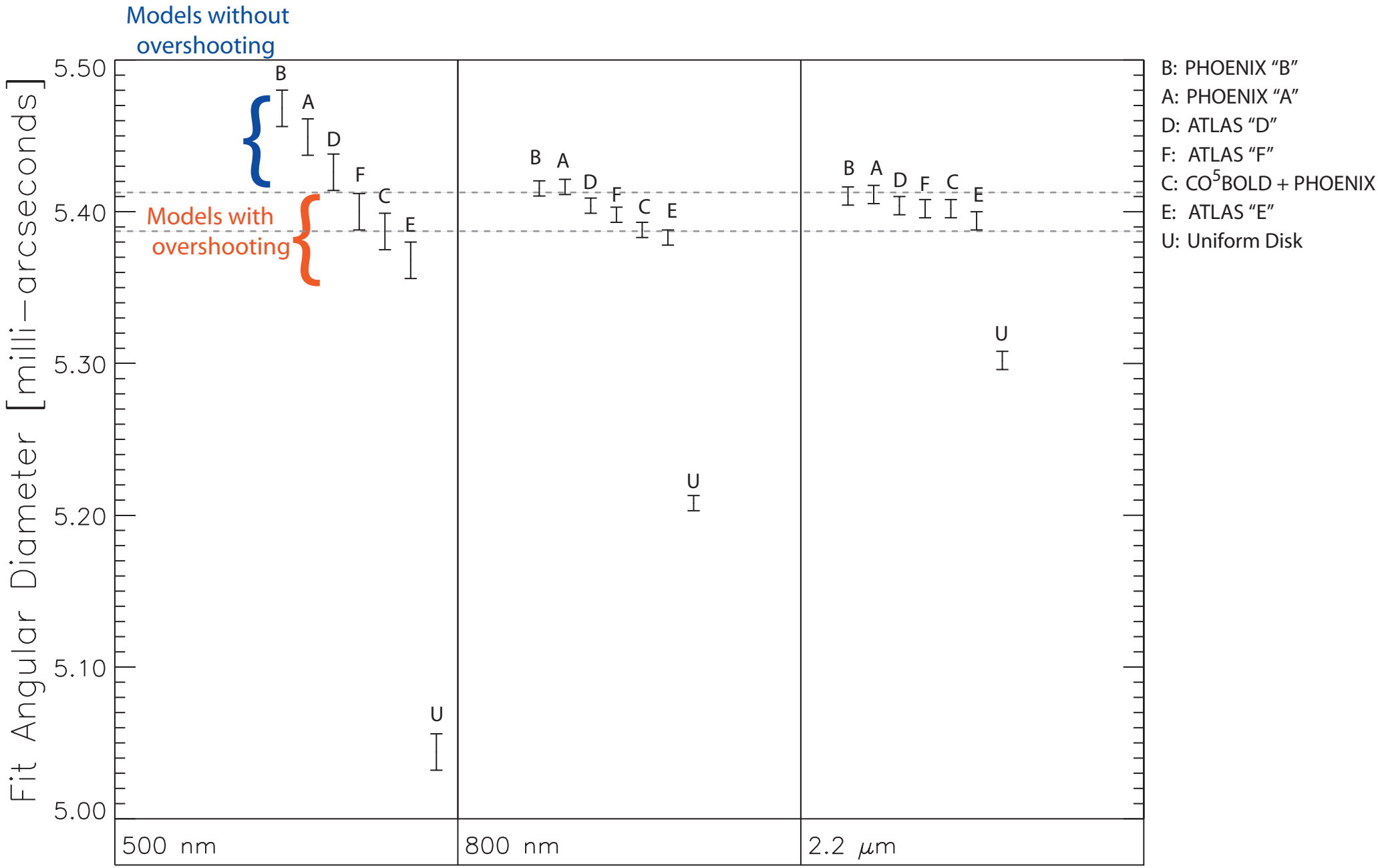

Comparing 1-D and 3-D Model Temperature Structures

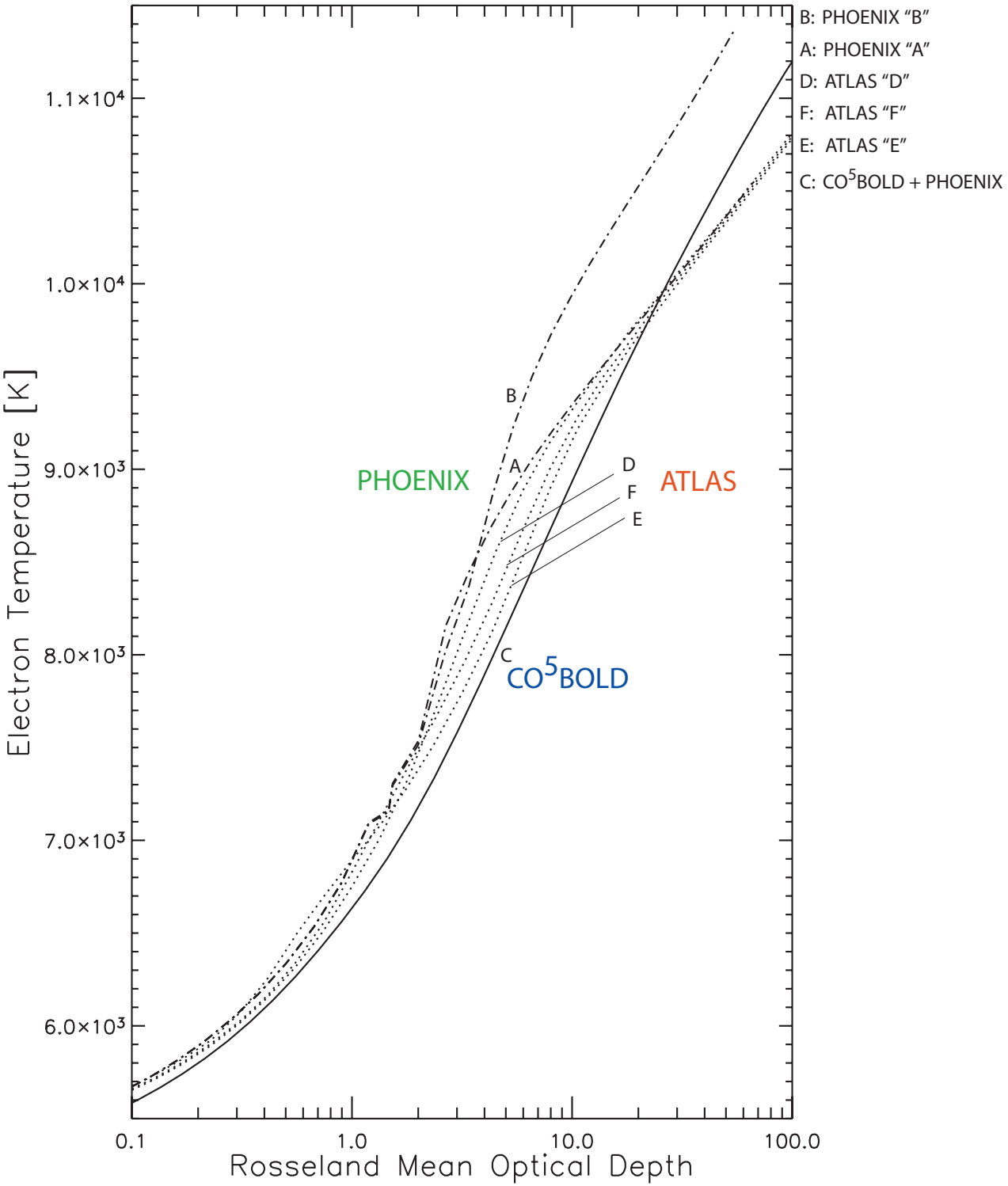

Wavelength-Dependent Opacity of the Solar-like Atmosphere

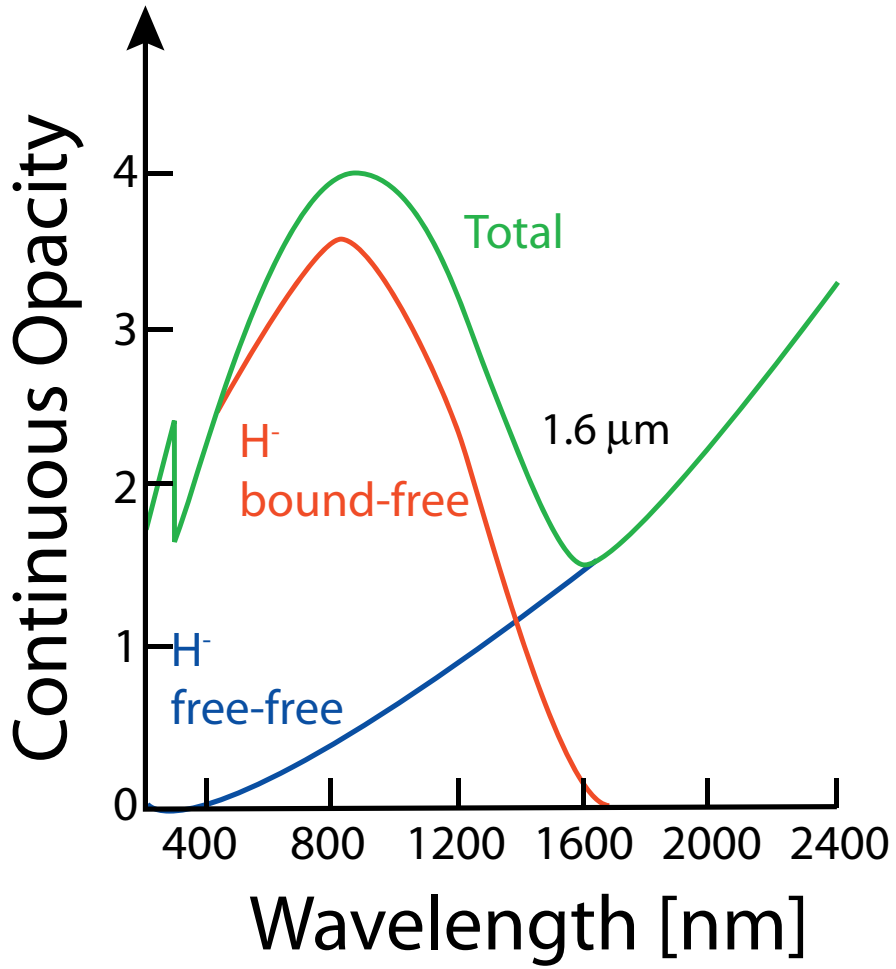

Summary

1. Interferometry is providing unique tests of multi-dimensional stellar atmosphere models

2. Beyond T_{eff} and log(g): gravity darkening, convection, winds, sphericity...

3. Vega: Rotating at ~91% of angular breakup rate; large 2500 K pole-to-equator gradient; convection at equator; debris disk sees cooler SED than we do.

$$\omega = \frac{\Omega}{\Omega_{\rm crit}} \not\equiv \frac{V_{\rm equ}}{V_{\rm crit}} = 2\,\cos\left[\frac{\pi + \cos^{-1}(\omega)}{3}\right]$$

4. Procyon: Limb darkening is convection-dependent; confirmation of 3-D model predictions; multi-wavelength measurements important for atmosphere analyses, go to the blue!

5. Next step: Testing atmosphere models with closure phases.